UNIVERSIDADE
BEIRA INTERIOR

Aerodynamic Analysis of a Two-Man Bobsleigh

(Versão Final Após Defesa)

Simão Rafael Silvério Ribeiro

Dissertação para obtenção do Grau de Mestre em
Engenharia Aeronáutica
(mestrado integrado)

Orientador: Prof. Doutor Pedro Vieira Gamboa

junho de 2025

Declaração de Integridade

Eu, Simão Rafael Silvério Ribeiro, que abaixo assino, estudante com o número de inscrição 43823 do Curso de Engenharia Aeronáutica da Faculdade de Engenharias, declaro ter desenvolvido o presente trabalho e elaborado o presente texto em total consonância com o **Código de Integridades da Universidade da Beira Interior.**

Mais concretamente afirmo não ter incorrido em qualquer das variedades de Fraude Académica, e que aqui declaro conhecer, que em particular atendi à exigida referenciação de frases, extratos, imagens e outras formas de trabalho intelectual, e assumindo assim na íntegra as responsabilidades da autoria.

Universidade da Beira Interior, Covilhã 12 / 06 / 2025

Dedicatória

Aos meus pais, que sempre me apoiaram incondicionalmente, me proporcionaram inúmeras oportunidades e fizeram vários sacrifícios ao longo do meu percurso académico. Sem o seu amor, dedicação e incentivo, nada disto teria sido possível.

À minha irmã, a quem eu vi crescer imenso durante este ano e de quem estou muito orgulhoso. A sua ajuda foi inestimável.

A toda a minha inúmera família, portuguesa e sem fronteiras, especialmente as minhas avós, que também tornaram tudo isto possível.

Aos meus amigos, tanto aos que criei na Covilhã e que passaram a ocupar um lugar especial no meu coração, como aos que me acompanham há mais tempo e a quem devo imenso.

À Mariana, que todos os dias me incentivou e com quem desejo crescer muito mais. Tenho mais sorte que juízo em te ter ao meu lado. ★

Agradecimentos

Agradeço especialmente ao Professor Pedro Vieira Gamboa, cujo conhecimento e dedicação foram fulcrais para a realização deste projeto. Estou profundamente grato pela sua disponibilidade e pelas suas valiosas sugestões, que tiveram um impacto significativo no seu desenvolvimento.

Agradeço ao Assistente Técnico João Manuel Laia Antunes pela ajuda a configurar a máquina remota e pela sua constante disponibilidade para me ajudar.

Agradeço ao Professor Francisco Miguel Ribeiro Proença Brójo pelos seus esclarecimentos e pelas sugestões que contribuíram para a melhoria deste trabalho.

Resumo

Bobsleigh é um desporto de inverno altamente competitivo, no qual os avanços tecnológicos desempenham um papel crucial na otimização do desempenho, sendo a aerodinâmica um fator determinante nos resultados das corridas. Este estudo apresenta uma análise aerodinâmica abrangente de um bobsleigh da categoria *2-man*, utilizando simulações de Dinâmica dos Fluidos Computacional (CFD) para investigar as caracterísitcas do escoamento e fontes de arrasto, com o objetivo de melhorar a eficiência aerodinâmica através de modificações à sua geometria.

Uma geometria de referência foi desenvolvida com base em referências fotográficas de designs de alto desempenho utilizados em competições recentes. As análises CFD foram realizadas no software ANSYS Fluent, empregando o modelo de turbulência Realizable $k - \varepsilon$ com Funções de Parede de Não-Equilíbrio para modelar a camada limite. Foram identificadas e estudadas características aerodinâmicas fundamentais, como regiões de separação e distribuições de pressão. As simulações foram realizadas para duas velocidades distintas do escoamento livre: 15 m/s, representativa da fase final do impulso inicial, e 35 m/s, correspondente à velocidade de corrida. Adicionalmente, foram efetuadas análises para avaliar a influência das paredes limitantes das secções retas da pista no desempenho aerodinâmico do bobsleigh.

Com base nestes resultados e em estudos prévios, foi conduzido um processo iterativo de melhoria geométrica para desenvolver um design melhorado com vista à redução do arrasto aerodinâmico. A nova geometria inclui modificações no bumper frontal, na distância da parte inferior da fuselagem ao solo e na geometria do difusor, resultando numa redução de 6,37% do arrasto aerodinâmico e num aumento de 3,14% da velocidade máxima.

Palavras-chave

Bobsleigh; Aerodinâmica; Coeficiente de Arrasto; Otimização; CFD

Abstract

Bobsleigh is a highly competitive winter sport in which technological advancements play a crucial role in optimising performance, with aerodynamics being a key factor in race outcomes. This study presents a comprehensive aerodynamic analysis of a two-man bobsleigh using Computational Fluid Dynamics (CFD) simulations to investigate flow structures and drag sources, with the objective of improving aerodynamic efficiency through geometric modifications.

A baseline bobsleigh geometry was developed using photographic references of high-performance designs from recent competitions. CFD analyses were conducted in ANSYS Fluent, employing the Realizable $k - \varepsilon$ turbulence model with Non-Equilibrium Wall Functions for near-wall modelling. Key aerodynamic characteristics, such as flow separation regions and pressure distributions were identified and studied. Simulations were performed at two distinct free-stream velocities: 15 m/s, representative of the late push start phase, and 35 m/s, corresponding to race-speed conditions. Additional analyses were conducted to evaluate the influence of confining walls in straight track sections on bobsleigh aerodynamic performance.

Based on these findings and existing research, an iterative design process was conducted to develop an improved geometry aimed at reducing aerodynamic drag. The enhanced design incorporates modifications to the front bumper, ground clearance, and diffuser geometry, resulting in a 6.37% reduction in aerodynamic drag and a 3.14% increase in maximum speed.

Keywords

Bobsleigh, Aerodynamics, Drag coefficient, Optimisation, CFD.

Contents

List of Figures

List of Tables

Acronyms

UBI	Universidade da Beira Interior
FDI-Portugal	Portuguese Winter Sports Federation
IBSF	International Bobsleigh and Skeleton Federation
CFD	Computational Fluid Dynamics
DNS	Direct Numerical Simulation
LES	Large Eddy Simulation
RANS	Reynolds-Averaged Navier-Stokes
SST	Shear-Stress Transport
CAD	Computer-Aided Design
CPU	Central Processing Unit
GPU	Graphics Processing Unit
FMG	Full Multigrid Method

Nomenclature

Re	Reynolds Number	
W	Total weight of the bobsleigh	$[N]$
θ	Descent slope angle	[°]
V	Relative flow speed	$[m/s]$
t	Time	$[s]$
F_N	Normal force	$[N]$
F_r	Resistive force	$[N]$
F_f	Ice friction force	$[N]$
F_D	Aerodynamic drag force	$[N]$
F_L	Aerodynamic lift force	$[N]$
ρ	Volumetric mass density	$[kg/m^3]$
C_D	Aerodynamic drag coefficient	
C_L	Aerodynamic lift coefficient	
A	Bobsleigh aspect ratio (frontal area)	$[m^2]$
μ_k	Kinetic friction coefficient	
m	Bobsleigh mass	$[kg]$
F_C	Centrifugal force	$[N]$
α	Corner slope angle	[°]
C_P	Pressure coefficient	
p	Local pressure	$[Pa]$
p_∞	Free-stream pressure	$[Pa]$
C_M	Coefficient of pitching moment	
M	Pitching moment	$[N\ m]$
u_i	Flow velocity directional component	$[m/s]$
x_i	Position directional component	$[m]$
U	Characteristic velocity	$[m/s]$
U_∞	Free-stream velocity	$[m/s]$
L	Characteristic length	$[m]$
μ	Dynamic viscosity	$[kg/(m\ s)]$
δ	Boundary layer thickness	$[m]$
τ	Shear stress	$[Pa]$
τ_w	Wall shear stress	$[Pa]$
y	Normal distance from the wall	$[m]$
ν	Kinematic viscosity	$[m^2/s]$
u^+	Dimensionless flow velocity	

u_τ	Friction velocity	$[m/s]$
κ	Von Kármán constant	
C^+	Log-law constant	
$\bar{u}$	Average velocity	$[m/s]$
u'	Fluctuating velocity	$[m/s]$
k	Turbulence kinetic energy	$[J]$
δ_{ij}	Kronecker delta	
μ_t	Turbulent viscosity	$[kg/(m\ s)]$
ε	Dissipation rate of turbulence kinetic energy	
ω	Specific turbulent dissipation rate	
B	Blockage ratio	
A_e	Control volume cross sectional area	$[m^2]$
T	Temperature	$[K]$
A_i	Control volume inlet cross-sectional area	$[m^2]$
V_i	Control volume inlet flow velocity	$[m/s]$
A_o	Control volume outlet cross-sectional area	$[m^2]$
V_o	Control volume outlet flow velocity	$[m/s]$

Chapter 1

1 Introduction

1.1 Motivation

Bobsleigh is a sport which heavily relies on technological advancement akin to Motorsports (Formula 1, MotoGP, etc.), Cycling or Swimming.

The margins of time by which the winners of a race are defined are extremely thin. In Bobsleigh, there have been cases where two teams shared the same podium place due to both finishing with identical times down to the hundredth of a second, as it happened with Canada and Germany, who saw a tie for the gold medal in the 2018 Winter Olympics, in Pyeongchang, South Korea. They were separated from Latvia, in third place, by 0.05 seconds. [1]

Participating teams are hence forced to constantly and actively research innovative and cutting-edge technology to increase their chances at success. The role of Aerodynamics is of the upmost importance since it is one of the most defining factors in gaining precious fractions of a second ahead of the competition.

To that end, a number of studies have been published investigating bobsleigh design strategies to achieve aerodynamic performance advantage, even if minimally. These works have focused on the optimisation of elements such as bumper geometry and placement [2], ground clearance [3], nose design [4], side wall contouring [5] and crew positioning [6]. Such studies have employed computational fluid dynamics (CFD), wind tunnel experiments, and prototype testing under real conditions on the track.

The insights gained from this body of research provide a foundational knowledge base for the present work, informing both the design decisions and methodological approach. This thesis continues the research initiated by Miguel Vasconcelos in *Estudo Aerodinâmico Preliminar de um Bobsled de 2 Lugares* [7], aiming to further develop a bobsleigh design proposal for *Bobteam Portugal*, a Portuguese bobsleigh team. The ultimate goal is to support the team's ambition to compete in the 2026 Winter Olympics.

1.2 Portugal in Bobsleigh

Portugal' debut in bobsleigh took place at the 1988 Winter Olympic Games, held in Calgary, Canada. The team was composed of António Reis, João Poupada, Jorge Magalhães, João Pires

and Rogério Bernardes, all Canadians of Portuguese descent, competing in the 2-man and 4-man categories. Portugal was not alone as a newcomer to the sport, since several other nations without strong bobsleigh traditions also made their Olympic debut in the sport. Such countries include Jamaica (whose participation became widely recognised, even today), Mexico, the U.S. Virgin Islands, New Zealand and the Netherlands Antilles. Despite participating in other international events, such as the Bobsleigh World Cup, no Portuguese bobsleigh team has returned to the Winter Olympics since its initial appearance. [8]

Bobteam Portugal is a more recent project under the Portuguese Winter Sports Federation (FDI-Portugal), aiming to return Portugal to Olympic bobsleigh competition at the 2026 Winter Games, to be held in Milan and Cortina d'Ampezzo, Italy (Figure 1.1). The team intends to compete in the 2-man category, with Raphaël Ribeiro as pilot and Abdel-Kadel Larrinaga as brakeman. [9]

Figure 1.1: Bobteam Portugal and FDI-Portugal logos [10]

To support this effort, Bobteam Portugal is developing an original cowling, collaborating with the University of Beira Interior (UBI), in order to conduct aerodynamic and structural studies aimed at optimising the cowling design.

1.3 Objectives

This work aims to improve the aerodynamic performance of a two-man bobsleigh, by developing an enhanced geometry following a comprehensive study of its associated flow phenomena, from macroscopic flow structures to wall-bounded flow behaviour. CFD simulations will be conducted and compared under different run conditions, for free-stream velocities of 35 m/s and 15 m/s, with and without the interference of confining walls, such as those present in the straight sections of bobsleigh competition tracks.

A CAD geometry is to be developed through photographic references of designs used by high-performance teams in recent competitions, ensuring a realistic representation of modern

bobsleigh geometry. This model will serve as the baseline for CFD simulations, allowing to identify key aerodynamic characteristics, separation zones and drag sources.

Subsequently, the study intends to present a structured methodology to improve the aerodynamic efficiency of a bobsleigh, applying techniques used in bobsleigh research and in other race vehicle aerodynamics. These design methods will be applied to a new bobsleigh geometry, designed to reduce aerodynamic drag, improving overall competition performance.

Finally, aerodynamic forces generated in each case will be compared, assessing the effects of geometry modifications and run conditions. The expected findings of this study aim to contribute to a greater understanding of bobsleigh aerodynamics and provide valuable insights for future design improvements in the sport.

1.4 Document Structure

The present work is divided in six main chapters, organised as follows:

- **Chapter 1:** Introduces the study subject, highlighting the importance of aerodynamic optimisation. Primary objectives of the research are defined.
- **Chapter 2:** Presents an overview of the sport of Bobsleigh, competition formats, historical background and technical concepts and nomenclature.
- **Chapter 3:** Discusses bobsleigh kinematics and aerodynamics principles, including key aerodynamic forces acting on the sleigh. Additionally, a review of the State-of-the-Art in the field is presented, summarising existing research hand technological advancements.
- **Chapter 4:** Describes the used computational approach, the development of the CAD model and CFD methodology, such as mesh generation, solver settings, and turbulence modelling. Geometric improvements of the *Enhanced Model* are also presented.
- **Chapter 5:** Aerodynamic results are analysed, where flow behaviour and drag contributions are studied and compared between geometries and run conditions.
- **Chapter 6:** Summarises the conclusions of the study. Additionally, proposes recommendations for future research in order to refine the understanding of bobsleigh aerodynamics.

Chapter 2

2 The Sport of Bobsleigh

2.1 Overview

It should be disclosed this report will focus exclusively on the 2-man category of bobsleigh. While many general concepts apply to bobsleighing as a whole, the other categories (4-man, 2-women and monobob) possess distinct nuances that differentiate them. The subsequent text will discuss technical concepts specific to 2-man category without any other notice.

A 2-man bobsleigh crew includes two members with distinct roles:

- **The driver (or pilot)** is tasked with driving the sleigh and ensuring optimal pathing along the track.
- **The brakeman:** is tucked behind the driver during most of the run, in the most aerodynamic way possible, helping in steering. When the run has concluded, the brakeman pulls the brakes, bringing the sleigh to a stop.

A bobsleigh run is initiated when the athletes start pushing the sleigh from a stationary position with explosive impulse to achieve maximum velocity. The driver grabs the retractable push bar and propels it for 20 to 30 metres, usually being the first loading into the sleigh (Figure 2.1). The brakeman grips the push handles in the rear of the bobsleigh during the push. As they accelerate beyond a speed at which the brakeman can keep pace (typically around 50 metres after the start), he boards the sleigh. (Figure 2.2). [11] [12]

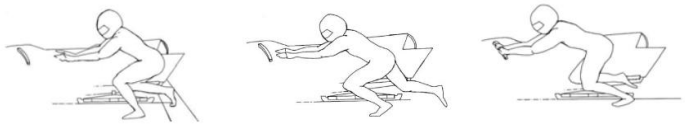

Figure 2.1: Driver's initial position and start of the push [12]

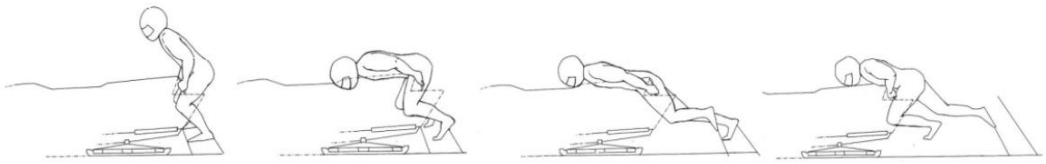

Figure 2.2: Brakeman's initial position and start of the push [12]

The clock starts once the crew reaches the 15-metre mark. The next photocell is found 65 metres after the start line. The time elapsed between these 50 metres is called the “start time”. This initial stage is crucial. A widely recognized rule of thumb dictates that a 0.01 s reduction in the start time is typically doubled or even tripled in the total time. [13] [14]

The start phase is followed by the drive. From this point until the end of the run, the only accelerating force acting on the sled will be gravity. [15]

The driver controls the direction of the bobsleigh’s front runners with a pulling-chord steering mechanism (Figure 2.3) and must navigate it along the track. His goal is to keep the optimal race line, particularly during corners, maintaining the sleigh high enough to conserve speed and engage the subsequent sections at an appropriate angle. Steering requires precise control, as adjusting the ropes by two or three centimetres rotates the runners by 10 or 15 degrees. Such adjustments must be carefully balanced, since it decelerates the sleigh and might lead it to travel a longer distance. Additionally, the driver must be cautious not to scrape the sides of the track, which also decelerates the sleigh and might hinder the team’s performance. [15] [16] [17]

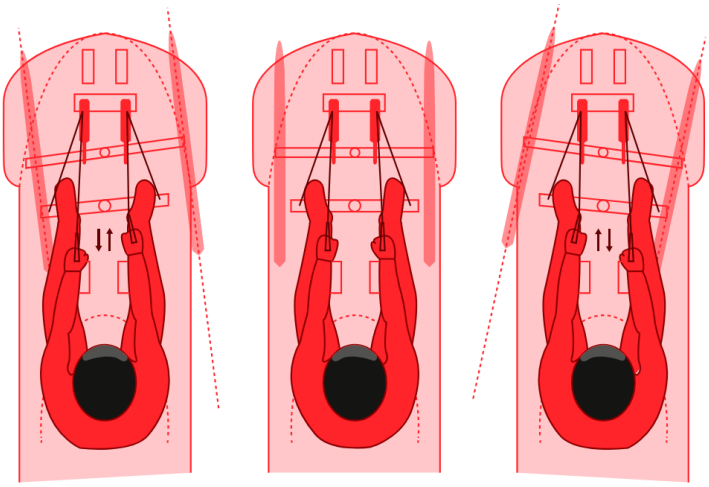

Figure 2.3: Steering mechanism of a bobsleigh [11]

During this stage, the brakeman is positioned behind the driver, maintaining an aerodynamic body shape to minimise aerodynamic drag. His role is to employ his weight to help steer the sleigh, bobbing his body during corners. This motion is characteristic of the sport and is the origin of its name. [15] [17]

2.2 History

Originating in the Swiss Alps during the 1880s, bobsleigh initially served as a thrilling pastime for wealthy locals and tourists who started racing in sleighs fitted with a steering mechanism.

However, the sport's appeal quickly transcended its regional roots, spreading across Europe and attracting both competitors and spectators. The term “bobsleigh” originated from the characteristic bobbing the crews would perform seeking to steer and accelerate their sleighs. [11]

St. Moritz, Switzerland saw the establishment of the world’s first bobsleigh club at the Kulm Hotel in 1897, an institution which remains active today. Just a year later, the club hosted the first organised competition (Figure 2.4). Several years later, in 1904, the first purpose-built bobsleigh track was opened. [18]

Figure 2.4: A bobsleigh competition held in St. Moritz (1918) [19]

The sport achieved international recognition with the founding of the *Fédération Internationale de Bobsleigh et de Tobogganing* in 1923, now known as IBSF (International Bobsleigh and Skeleton Federation), and with its inclusion in the following year’s edition of the Olympic Winter Games, in Chamonix, France. During this era, professional competitors were non-existent, neither was regular training regimens. Teams were comprised of enthusiasts who would either rent or purchase their sleighs and start competing.

With growing popularity, Bobsleighing, as we know it today started taking shape in the mid-20th century, when several efforts were made to standardise the sport, making it more competitive and safer:

- **The total weight limit was significantly lowered**, forcing a radical shift in team strategies, who sought to increase descent speeds by maximizing the sleigh's overall mass. Sleigh design underwent a significant transformation, becoming heavily dependent on aerodynamics and materials science research, shifting towards more streamlined bodies

and smoother surfaces to reduce air resistance, built with advanced composites like carbon fibre and fibreglass, making them lighter yet more durable. [20]

- **Tracks were regularised**, departing from the rudimentary, highly variable paths often carved out of natural ice down snowy hillsides. Artificial tracks with refrigeration systems began to be constructed, eliminating the dependence on fluctuating weather conditions. These tracks were designed with greater precision, incorporating more technical sections to test the skill of pilots and the aerodynamic capabilities of the sleds. [21]
- **Crews became more athletic,** refining their form and coordination during the push start. They started being drawn from other sports, such as track and field, handball and gymnastics, enabling them to deliver agility and explosive force in this crucial phase and shave precious milliseconds off their run time. [11]

2.3 The Sleigh

This section aims to familiarise the reader on essential bobsleigh terminology which will be used extensively throughout the report. Certain internal structural components, such as the steel frame are omitted from this discussion due to their limited relevance in aerodynamic studies, as they do not interact with the external airflow. The terms shown in the labelled diagram in Figure 2.5 are commonly utilised by athletes, designers, regulatory authorities and in scientific literature. The specific bobsleigh components introduced will be analysed in terms of their function and typical variations. Their shape and dimensions are subject to extensive IBSF regulations [22], which impose significant restrictions on design and manufacturing modifications.

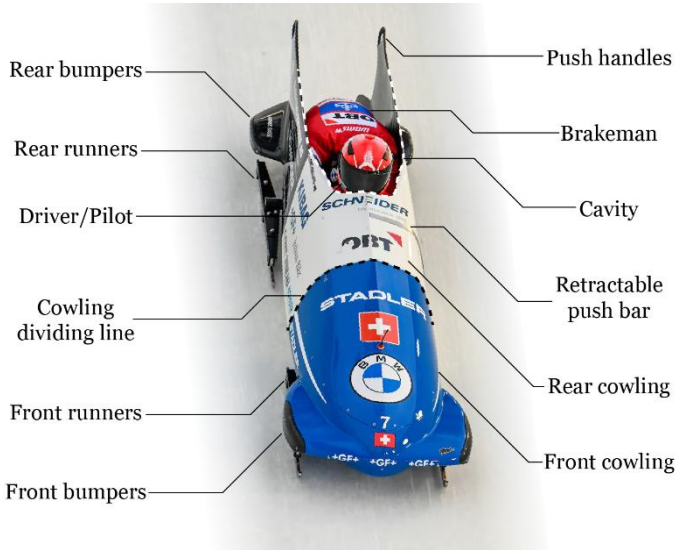

Figure 2.5: Nomenclature of several parts of a 2-man bobsleigh (photograph sourced from [23])

The cowling is the main body of the sleigh, often called fuselage or hull, housing the athletes during the race and providing crucial protection in the event of a crash. It plays a significant role in aerodynamics, as most smooth surfaces designed to minimise turbulent effects are located here. The cowling is hollow and of convex shape, extending from the nose to the open rear. It is typically constructed of fibreglass and composed of two separate sections: the front cowling and the rear cowling.

The cowling dividing line is a visible slit which separates its movable front section from its fixed rear section. This gap may be left open, although usually teams cover it with a rubber strip to reduce flow separation and improve aerodynamic efficiency. [24]

The runners are the only contact point with the ground in normal circumstances. They must be constructed from a standardised steel, distributed by IBSF, with no plating or coating permitted. At the start of the race, the runners must be at ambient temperature to prevent unfair reductions in runner-ice friction. They are mounted on the steel frame, inside the cowling. The front runners are connected to the pivotal joint in the front cowling, allowing it to steer along with it.

The bumpers, although wing-like in appearance, don't have any lift-generating purpose [25]. Their only functions are that of absorbing impacts with the edges of the track, protecting the sleigh and crew, and that of preventing the runners from scraping against the side walls. Design regulations for bumpers are relatively flexible, permitting a range of approaches.

The push bar and push handle transfer the athletes' traction to the sleigh during the initial push start. Once the driver stops pushing and board the sleigh, the side bar is retracted to prevent it from interfering with aerodynamic performance.

2.4 Tracks

All modern IBSF-homologated tracks are subject to strict regulations to ensure the safety of participants and spectators. These regulations also serve to standardise the sport by controlling the level of technical difficulty and maintaining consistent environmental conditions.

Bobsleigh runs range from 1200m and 2000m, with a slope angle varying of about 8-15%. A standard track must include a minimum of thirteen curves and is divided into three sectors, which should not be mistaken with the three phases of a race (push start, descent, finish). These sectors delimit track design elements along the race [26]:

- **1st sector (Acceleration):** The initial 350–400 meters include a limited number of curves, and the slope gradient increases gradually to facilitate acceleration

- **2nd sector (Maximum Performance):** This sector, typically 800–850 meters in length, contains the majority of the curves, with the slope gradient reaching its steepest point to allow for maximum speed
- **3rd sector (Active Finish):** In the final sector, the slope gradient and the number of curves is reduced. This segment must feature a "labyrinth" element, which is a series of three or more consecutive curves

There are currently sixteen bobsleigh tracks worldwide that meet international standards for competition. Figure 2.6 presents the layouts of three different bobsleigh tracks, showcasing how much they might differ.

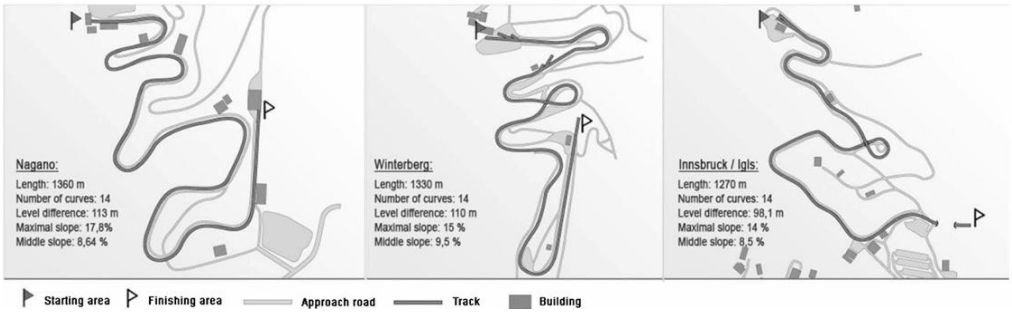

Figure 2.6: Schemes of three different bobsleigh tracks and corresponding specified characteristics [26]

Chapter 3

3 Literature Review

3.1 IBSF Regulations

The IBSF annually publishes the **International Bobsleigh Rules** compendium [22], specifying and regulating several aspects of the sport:

- Competitions and disciplines
- Admission criteria and rights to participate in competitions
- Guidelines for event organisation
- Nomination and authority of jury members and officials
- Competition regulations
- Medical requirements and technical inspections
- Advertising guidelines and rule enforcement
- Material acquisition
- Equipment design and construction

The last two categories are particularly relevant to the practical aspects of bobsleigh manufacturing, as they aim to ensure:

- Resistance of materials to the stresses of training and competition
- Adequate protection for participants and spectators
- Preservation of track integrity
- Fair and honest competition
- Fair limit on the cost of equipment

This document is the regulation guidebook for any team participating in any official IBSF event. Respecting these regulations is mandatory for all participating teams during the development of their designs. The bobsleigh models analysed in this work also respect these regulations, namely in equipment design, ensuring a practical applicability of its findings.

3.2 Fundamentals of Bobsleigh Aerodynamics

3.2.1 Forces at Play

When setting out to build a bobsleigh for competitive purposes, one must pay close attention to the several forces acting on it during the run. They will affect everything from stability, safety and speed.

In the starting phase of the run, athletes are required push the sleigh from a stationary position and gain as much speed as possible in a short period of time. In these conditions, aerodynamic considerations are relatively insignificant due to the substantially reduced speed. Instead, the athletes' explosive pushing force and the friction in the sleigh runners and the athletes' cleats play a bigger role in generating the necessary momentum. For this reason, this report will focus exclusively on the descent, where aerodynamic forces become a vital factor.

During the descent, the contestants are already positioned within the bobsleigh. Their role shifts from pushing it forward to drive it effectively through the track (the driver steers while the brakeman bobs his body to help in steering). As previously noted, once the crew is inside the sleigh, the only force positively accelerating it will be gravity. Figure 3.1 shows the forces acting on a bobsleigh during a straight section in the descent.

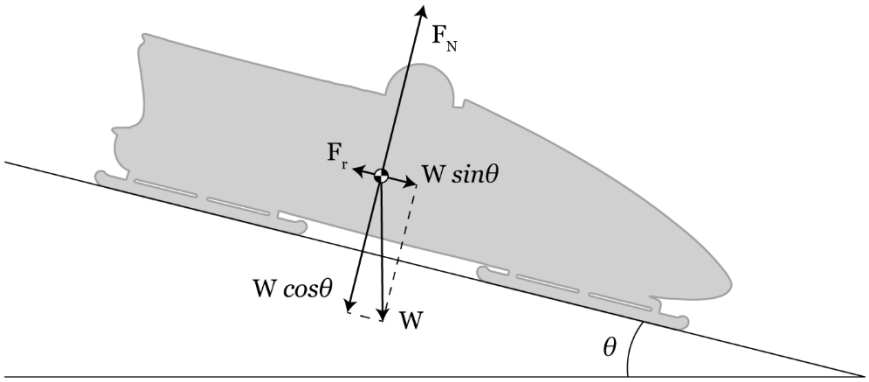

Figure 3.1: Forces acting on a bobsleigh during a straight section (image provided by the author, adapted from an illustration in [27])

Using this simple model of forces, one can compute the resulting force in the longitudinal axis, taking in account resistive forces:

$$m\frac{dV}{dt} = W\sin\theta - F_r \tag{3.1}$$

where m is the total mass of the bobsleigh, V is the speed of the bobsleigh, t is time, W is the total weight of the bobsleigh, θ is the slope angle and F_r is the resistive force.

The total resistive force can be decomposed into aerodynamic drag and ice friction ($F_r = F_D + F_f$):

$$F_D = \frac{1}{2}\rho C_D A V^2 \tag{3.2}$$

$$F_f = \mu_k(W\cos\theta - F_L) \tag{3.3}$$

where ρ is the air density, C_D is the drag coefficient, A is the frontal area of the bobsleigh, μ_k is the kinetic friction coefficient and F_L is the lift force.

In Equation (3.2), F_D is dependent on C_D, the term for drag coefficient. This and other force coefficient are discussed in Chapter 3.2.2.

The lift magnitude is defined as positive when pointing upward, opposing the normal contribution of weight. Lift generated by bobsleighs is usually negative, increasing the sled's runners friction with the ice. However, its impact in bobsleigh aerodynamics is minimal, and in the case of some simplistic models, it is often neglected. Nevertheless, minimising its magnitude is beneficial for reducing ice friction. Additionally, a reduction of lift generation inherently reduces lift induced drag, which correlates to a reduction in total drag [27]. Further explanation on drag reduction will be presented in Chapter 3.2.2.

The forces acting normally to the incline are related as follows:

$$F_N = W\cos\theta - F_L \tag{3.4}$$

$$F_L = \frac{1}{2}\rho C_L A V^2 \tag{3.5}$$

where C_L is the lift coefficient.

Using the equations presented, Sabbioni et al. [27] developed a simple mathematical model to evaluate how the performance of a bobsleigh was affected by several parameters over the course of a run. For the purpose of this model, the track was considered to be a 1500-metre straight slope with constant incline and no corners, simplifying the analysis. Each parameter was increased in 10%, from a reference value, to determine how much they impacted the final run time. Their relative contributions to the performance are illustrated in Figure 3.2.

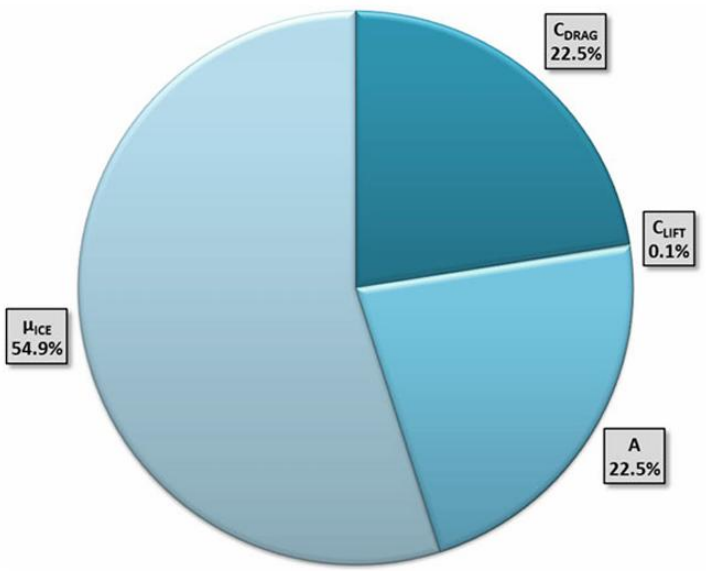

Figure 3.2: Relative impact of parameters on bobsleigh performance [27]

As shown in Figure 3.2, the parameter with the greatest relative impact on the final run time is the kinetic ice friction coefficient, with more than two times the influence of any other. Its value suffers negligible fluctuations during a run and is thus considered constant [25]. Lift generation affects ice friction force, although insignificantly. Therefore, ice friction force can also be considered constant during straight sections as it is dependent from μ_k and vertical forces (Equation (3.3)). This assumption, however, is only valid when considering the track to be a straight slope. It cannot be applied in corner sections where inertial effects, countering the turning motion, will greatly increase downward vertical forces and considerably increase ice friction.

In bobsleigh tracks, the course becomes nearly vertical in most curves, permitting the athletes to navigate them without the need for excessive braking, preserving the high speeds characteristic of the sport without sacrificing technical difficulty. When in a corner, the force set-up is comparable to that of a *Well of Death* attraction, as seen in festivals in Northern India [28] (Figure 3.3). In both cases, the effects of inertia oppose the rotation motion, pressing the vehicle against a nearly vertical surface. This increases the frictional force generated by wheels or runners, which will counter the gravitational pull, allowing the vehicle to maintain its altitude along the curve.

Figure 3.3: Comparison between "Well of Death" Indian attraction (left) and a bobsleigh traversing a curve section (right) [28] [29]

In Figure 3.4, the aerodynamic drag force is considered normal to the plane of reference, thus not shown in the picture as it would represent an out-of-plane force. Additionally, for simplification purposes, the force diagram uses the bobsleigh itself as a non-inertial reference frame. To account for the effects of inertia and the consequent acceleration of the reference frame, a centrifugal force (F_C) is inserted, acting on the sleigh directed away from the centre of the circle of motion. According to IBSF regulations, athletes may be exposed to a maximum centrifugal force of 5G, which can be sustained continuously for no more than two seconds [30]. Therefore, the scenario depicted represents an extreme case.

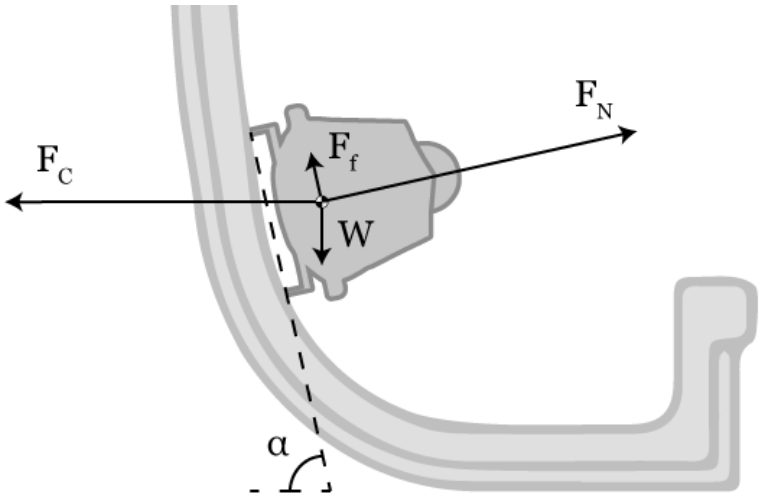

Figure 3.4: Forces acting on a bobsleigh during a corner at 5G (image provided by the author; corner geometry based on an illustration in [26])

The forces are related in the following manner:

$$F_N = W\cos\alpha + F_C\cos\left(\frac{\pi}{2} - \alpha\right) \tag{3.6}$$

$$F_f = \mu_k F_N = \mu_k\left[W\cos\alpha + F_C\cos\left(\frac{\pi}{2} - \alpha\right)\right] \tag{3.7}$$

Where α is the corner slope angle.

As demonstrated, the friction of the sleigh runners with ice can only be considered constant on straight sections of the track. To calculate a realistic run time, an effective approach is to model the track as a straight slope while incorporating an additional constant factor to address the influence of extra friction on curve sections on overall time, as done in [25].

Although the friction of the sleigh runners with ice substantially impacts performance and plays a crucial role in enhancing it, the main focus of this report is more closely related with the remaining parameters with great impact: aerodynamic drag coefficient and frontal area. Both these factors directly influence drag generation and should be minimised as much as possible.

3.2.2 Aerodynamic Drag Generation and Reduction

Drag forces acting on a bobsleigh arise from multiple sources and can be classified into two primary categories: induced drag and parasite drag.

Induced drag is an inevitable consequence of lift production and, as stated in Chapter 3.2.1, can be minimised by reducing lift forces. This type of drag results from pressure differentials that occur on downforce generating surfaces. However, its impact is limited in bobsleigh aerodynamics as lift magnitude is relatively small and is even reduced as speed increases. [25]

Parasite drag, on the other hand, is the predominant form of drag during the race and intensifies with increasing speed. Unlike induced drag, parasite drag is not related to lift; rather, it arises from the interaction between the bobsleigh's shape and the oncoming airflow. Its main component is pressure drag , which accounts for at least 60% of total drag in bluff bodies, like a sleigh [24]. Pressure drag is caused by the separation of the boundary layer from the bobsleigh's surface contours, forming wakes and negative pressure gradients behind protruding components (bumpers, runners, axles, cowling, driver's helmet, …).

A second source of parasite drag is called skin friction drag, caused by shear forces from the deceleration of the airflow along the bobsleigh's surface. Its magnitude is intensified by the roughness of certain surfaces, such as rivets and ridges. To minimise this effect, all surfaces must be as smooth as possible to reduce resistance.

Four force coefficients worthy of note are widely used when designing immersed bodies:

- **Drag coefficient**, C_D, is a non-dimensional quantity which measures drag-producing capabilities of an immersed body shape, generalising them for any flow conditions and sizes, as shown in Equation (3.8).

$$C_D = \frac{F_D}{\frac{1}{2}\rho V^2 A} \tag{3.8}$$

- **Lift coefficient**, C_L, is comparable to drag coefficient, only measuring lift generation instead of drag.

$$C_L = \frac{F_L}{\frac{1}{2}\rho V^2 A} \tag{3.9}$$

- **Pressure coefficient**, C_P, describes the relative pressure of a given point in the flow field, p, comparing it with free-stream pressure, p_∞.

$$C_P = \frac{p - p_\infty}{\frac{1}{2}\rho V^2} \tag{3.10}$$

- **Pitching moment coefficient**, C_M, measures the moment produced by aerodynamic forces with respect to the aerodynamic centre.

$$C_M = \frac{M}{\frac{1}{2}\rho V^2 A L} \tag{3.11}$$

where M is the pitching moment and L is the characteristic length.

The primary approach to reduce aerodynamic drag involves minimising both the drag coefficient and the frontal area. This task is challenging due to the constraints imposed by IBSF regulations and to the fact that occasionally drag coefficient and the frontal area contradict each other, requiring designers to find an optimal balance. [24]

Another significant hurdle in drag reduction is the cavity at the top of the cowling. This cavity causes flow separation at its trailing edge, generating a delta wing vortex, characterized by high rotational velocities and negative pressure coefficient regions, leading to increased drag. This phenomenon is illustrated in Figure 3.5.

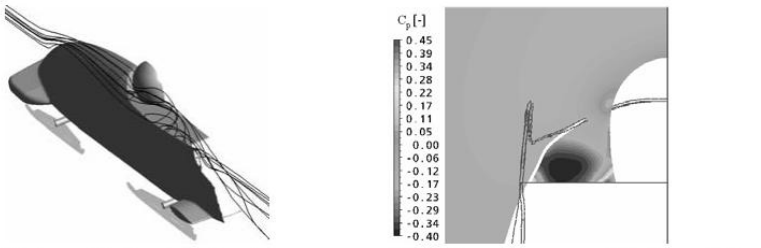

a) Vortex evolving from the leading edge. **b)** Back view on the pressure coefficient at x_1 = 1,65 m.

Figure 3.5: Vortex evolving from the leading edge of the cavity [24]

Lewis [25] provides a comprehensive calculation of the drag coefficient for each major bobsleigh component to estimate drag contribution for each of them. A summary of these findings is presented in Figure 3.6.

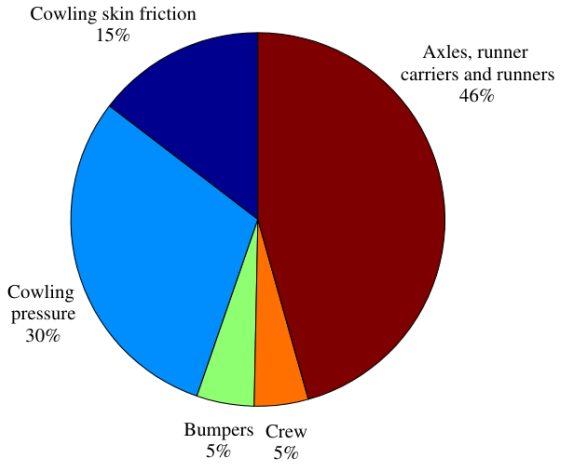

Figure 3.6: Relative drag contribution of bobsleigh components [25]

As expected, the cowling and runner system are responsible for the majority of drag as they are in direct contact with the airflow and possess relatively large surface areas. However, bumpers and crew contributions are also significant, presenting viable targets for performance optimisation.

Lewis further highlights, in agreement with several other researchers, that implementing flow stabilising and vortex generating surfaces such as strakes, trailing edge notches or splitter plates would be welcome in improving bobsleigh performance but are strictly forbidden by the IBSF Rule Book [22].

3.3 Turbulent Flows

3.3.1 Turbulent Flow Characteristics

Turbulence is a regime of fluid flow characterised by chaotic and unsteady motion, generally resulting from disturbances caused by interactions with solid surfaces or other flow streams. Due to its irregular nature, the precise prediction of flow parameters such as velocity, pressure or temperature at specific spatial and temporal coordinates becomes impossible. Despite these random fluctuations, turbulence can be rendered through statistically averaged values, enabling the prediction of its behaviour.

A key characteristic of turbulent flow is vorticity. This mechanism generates large scale three-dimensional eddies, which contain the majority of the kinetic energy of the flow. These structures are broken down into progressively smaller vortices until they reach critically small scales (known as the Kolmogorov microscales) in which the kinetic energy will be dissipated and converted into thermal energy, thanks to viscous shear stresses in the fluid. Turbulent flows are also distinguished by their capacity of transport and mixing increased rates of momentum, heat, and mass. [31]

In contrast, laminar flow is defined by the absence of turbulence. Its flow patterns are organised, characterised by smooth streamlines, parallel to each other. Flow properties remain uniform across both time and space dimensions, allowing for a precise prediction. [32]

3.3.2 Reynolds Number

The Reynolds number is a non-dimensional parameter which determines flow behaviour through a ratio between the magnitudes of inertial and viscous forces. It is defined as:

$$Re = \frac{\rho U_\infty L}{\mu} \tag{3.12}$$

where U_∞ is the free-stream velocity and μ is the dynamic viscosity.

A high Reynolds number indicates a dominance of inertial forces over viscous forces, leading to a turbulent regime. However, the value at which the transition from laminar flow occurs is case-dependent. In pipes and other enclosed systems, it occurs approximately at $Re \approx 4200$, while in free-stream flows over a flat plate, the critical value can reach as high as $Re \approx 500{,}000$. [32]

3.3.3 Navier-Stokes Equations

The Navier-Stokes Equations are used as a fundamental basis to describe the relationships among velocity, pressure, temperature and density in a moving fluid. These equations are a non-linear

coupled differential system with limited practical applications due to their complexity. As a result, numerical solutions obtained through computational grid-based methods, such as finite volume and finite difference techniques, are typically employed to solve them. [32]

In the present case study, to simplify these equations, it is acceptable to consider the fluid flow to be Newtonian, incompressible and isothermal. These assumptions render the fluid's dynamic viscosity (μ) and density (ρ) constant, unaffected by any external forces.

Under these conditions, the Navier-Stokes Continuity and Momentum Equations, respectively, can be written in Cartesian tensor form as follows:

$$\frac{\partial u_i}{\partial x_i} = 0 \tag{3.13}$$

$$\frac{\partial u_i}{\partial t} + u_j \frac{\partial u_i}{\partial x_j} = -\frac{1}{\rho}\frac{\partial p}{\partial x_i} + \mu \frac{\partial^2 u_i}{\partial x_j^2} \tag{3.14}$$

where u is flow velocity and x is position. The i notation represents directional components while the use of the j notation implies summation over all directions.

3.4 Boundary Layer Theory

The boundary layer is the region of a fluid flow adjacent to a surface when moving past an object. The fluid particles closest to the boundary suffer frictional resistance, adhering to its surface, acquiring the same velocity as the boundary itself. This phenomenon is known as no-slip condition. This interaction greatly disturbs the fluid's motion in the near-wall area, as shear stresses, resulting from the fluid's viscosity and wall friction, cause the relatively stationary particles to drag neighbouring sub-layers, thereby generating a velocity gradient in the region. The boundary layer comprises the portion of the fluid affected by the presence of the boundary, characterised by different velocities from those on the undisturbed free-stream. [33]

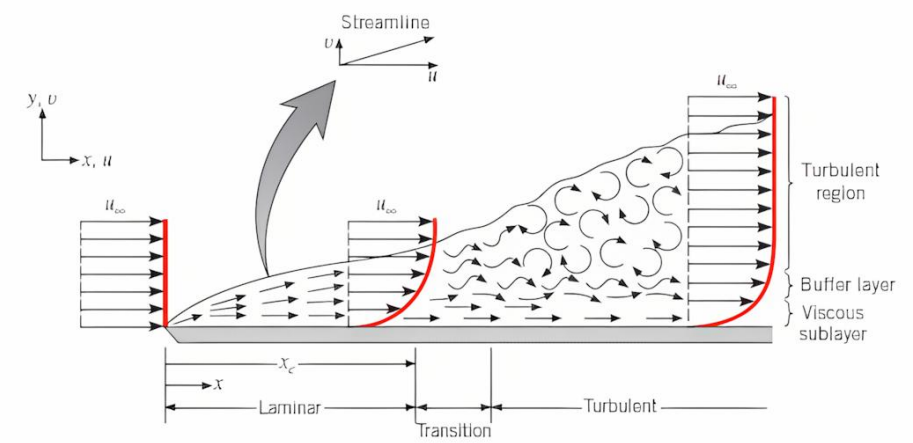

Figure 3.7: Velocity boundary layer in a flat plate [34]

3.4.1 Streamwise Direction

Figure 3.7 depicts a phenomenon known as boundary layer transition. A boundary layer typically starts out as laminar in the leading edges of the immersed object, adhering to its surface. However, if developing further downstream in its surface, the boundary layer eventually becomes turbulent, given the Reynolds number is high enough. In this case, a distinct transition region can be outlined. Here the flow starts developing instabilities which will eventually lead to a turbulent regime.

Accurately predicting boundary layer transition is crucial for modelling flow behaviour, as it directly affects aerodynamic performance. Since different turbulence closing models have different methods to calculate separation, transition and near-wall effects with varying degrees of accuracy, using the appropriate models for each situation is critically important in obtaining reliable simulations.

In the streamwise direction, shear stress, τ, is applied throughout the boundary layer. The fluid particles closest to the surface experience the highest shear stress, referred to as wall shear stress, τ_w [33]. This stress is directly proportional to the velocity gradient at the wall as shown:

$$\tau_w = \rho\nu\left(\frac{d\bar{u}}{dx}\right)_{y=0} \tag{3.15}$$

where $\bar{u}$ is the average velocity, y is the normal distance form the wall and kinematic viscosity, ν, is defined as:

$$\nu = \frac{\mu}{\rho} \tag{3.16}$$

Shear stress is transmitted to fluid particles and gradually dissipates in the direction normal to the flow. This dampening continues until the free-stream, where the influence of shear stresses caused by the wall is negligible.

Another important parameter is the dimensionless flow velocity, u^+, which characterises streamwise flow velocity in a generalised form, applicable to any flow conditions. Similarly to force coefficients, it is useful for comparing different scenarios. Dimensionless flow velocity is defined as:

$$u^+ = \frac{u}{u_\tau} \tag{3.17}$$

where friction velocity, u_τ, is defined as:

$$u_\tau = \sqrt{\frac{\tau_w}{p}} \tag{3.18}$$

3.4.2 Normal Direction

The normal direction to the flow is typically characterised using the dimensionless wall distance, y^+, which is employed similarly to u^+. It is calculated as:

$$y^+ = \frac{y u_\tau}{\nu} \tag{3.19}$$

Near-wall velocity distribution in this direction is usually predicted using the Law of the Wall. This is an assumption that turbulence near the boundary is only dependent on local conditions and is unaffected by flow motion further away and follows the same rules for nearly all flows. [33]

As illustrated in Figure 3.7, three distinct regions can be identified in the normal direction. Each region delimiting where the Law of the Wall governing equations can be accurately applied:

- **Viscous sublayer** ($y^+ < 5$)**:** viscous effects prevail over shear stress caused by the free-stream. The effects of the number of Reynolds are negligible. A linear relationship exists between the dimensionless quantities:

$$u^+ = y^+ \tag{3.20}$$

- **Logarithmic layer or log-law region** ($y^+ > 30$)**:** turbulence stresses become dominant, and the velocity profile exhibits a slow variation along the normal direction. The relation between dimensionless quantities is given by:

$$u^+ = \frac{1}{\kappa} \ln(y^+) + C^+ \tag{3.21}$$

where κ is the von Kármán Constant and C^+ is the log-law constant. Their values are not consistent throughout the literature but can be considered to be within 5% of the following values [33]:

$$\kappa = 0.41, \qquad C^+ = 5.2 \tag{3.22}$$

- **Buffer layer** $(\mathbf{5 < y^+ < 30})$**:** as a transition region, neither viscous nor turbulent effects clearly dominate. Instead, both have similar magnitudes, making the flow less well-defined.

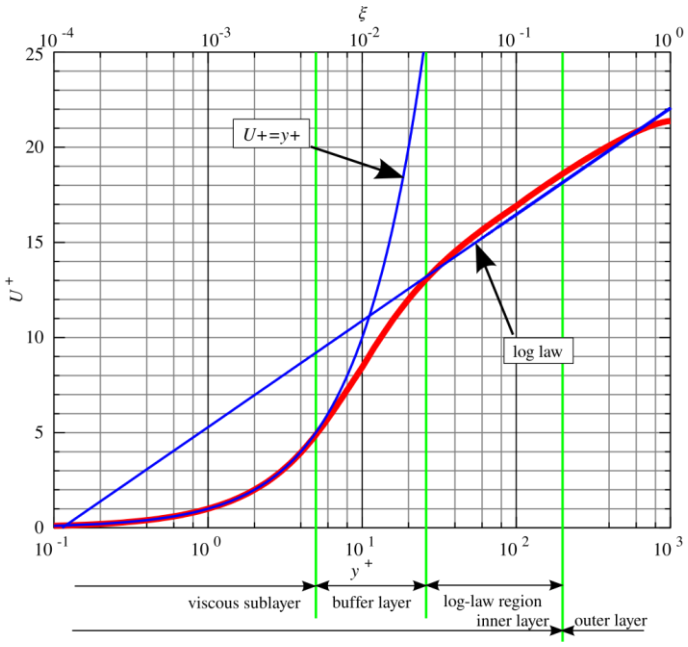

Figure 3.8: Law of the Wall regions and equations [35]

Figure 3.8 provides a graphical representation of the Law of the Wall regions and their equations, showing an outer layer of the flow, where these equations are not applicable. As the velocity in the log-law region has a slow vertical variation, the transition to the outer region is not well defined and varies depending on specific flow scenarios. Additionally, the figure compares the theoretical velocity functions for the viscous sublayer and log-law region (depicted in blue) with empirical data for the velocity profile in a turbulent boundary layer (depicted in red). This comparison further illustrates the limitations of Law of the Wall, as neither the linear nor the logarithmic functions accurately predict the velocity gradient in the buffer layer.

3.4.3 Turbulence Modelling

The advent of CFD has made it possible to solve the Navier-Stokes equations and predict the evolution of most turbulent flows. This advancement complements practical applications as mean or statistical values for the flow properties are sufficient and are considered a reliable solution. Several modelling approaches are available, with varying degrees of freedom, which increases computational cost. The choice of approach significantly impacts the geometric complexity that can be efficiently resolved. Turbulence models can be categorized into the following types:

- **Direct Numerical Simulation (DNS):** Solves the Navier-Stokes equations directly across all spatial and temporal scales, capturing all flow behaviour for a specific instance in time. Its high computational cost forces it to have limited applications, only being employed in in simple geometries, for low-to-moderate Reynolds numbers. While included in this list, DNS is a form of turbulent-flow simulation rather than a turbulence model. [33]
- **Large Eddy Simulation (LES):** Solves high eddy scales, where most of the energy transfer occurs, filtering out the the smaller scales. The stresses in scales smaller than the mesh size are modelled, with approximate levels of these stresses being determined. While increasing the range of applicability, offering a balance between accuracy and computational efficiency, LES is still too resource-intensive to be widely used. [37]
- **Reynolds-Averaged Navier-Stokes (RANS):** Models all the turbulence scales, obtaining a simplified representation of flow behaviour through averaged values. This approach has the most widespread use in all kinds of applications due to its efficiency, despite its inherent loss of accuracy. [37]

RANS methods are the most well-suited to efficiently solve the flow over the complex geometry of a bobsleigh and are regarded as the standard approach among researchers in the field.

3.5 Computational Fluid Dynamics

The field of theoretical fluid dynamics has been evolving, as recognised today, has evolved since the eighteenth century. Despite this long history, the complexity of flow problems initially forbade the formulated equations from being effectively solved and applied to practical fluid dynamics analyses. The development of high-performance digital computers, combined with accurate numerical methods permitted a new complementary approach: computational fluid dynamics (CFD).

Nowadays, CFD has become an invaluable tool for research and development, enabling the prediction and analysis of fluid flows based on governing equations, such as the Navier-Stokes

equations. Compared to purely theoretical and experimental approaches, CFD excels through its flexibility, time and cost effectiveness and unparalleled flow data monitoring capabilities. [36]

3.5.1 RANS Turbulence Models

Reynolds averaging decomposes flow properties into the averaged and the fluctuating components. The turbulence fluctuation for velocity is:

$$u_i = \bar{u}_i + u_i' \tag{3.23}$$

where u' is the fluctuating velocity term.

Substituting the velocity terms from Equation (3.23) into Equations (3.13) and (3.14) produces the Reynolds-averaged Navier-Stokes equations:

$$\frac{\partial \bar{u}_i}{\partial x_i} = 0 \tag{3.24}$$

$$\frac{\partial \bar{u}_i}{\partial t} + \frac{\partial}{\partial x_j}\left(\overline{u_\iota u_j}\right) = -\frac{1}{\rho}\frac{\partial \bar{p}}{\partial x_i} + \mu\frac{\partial^2 \bar{u}_i}{\partial x_j^2} - \frac{\partial}{\partial x_j}\left(\rho\overline{u'_\iota u'_j}\right) \tag{3.25}$$

RANS equations have the same general form as instantaneous Navier Stokes, with solution variables represented as time-averaged values. They also contain an additional term $\left(\rho\overline{u'_\iota u'_j}\right)$, known as Reynolds Stresses, accounting for the effects of turbulence. They must be modelled to close Equation (3.25). A common method for this is the Boussinesq Approach, an approximation for turbulent viscosity which assumes a linear relationship between turbulent or Reynolds Stresses and the mean strain rate. It can be expressed as:

$$\rho\overline{u'_\iota u'_j} = \frac{2}{3}\rho k\delta_{ij} - \mu_t\left(\frac{\partial \bar{u}_i}{\partial x_j} + \frac{\partial \bar{u}_j}{\partial x_i}\right) \tag{3.26}$$

where δ_{ij} represents the Kronecker delta, a mathematical two-variable function employed in the Boussinesq Approximation definition. It should not be confused with δ, boundary layer thickness, the relative height from the wall at which the flow transitions from the boundary layer to the free-stream. [37]

Some of the most used turbulence models in industrial applications are Boussinesq-based RANS models. The most prominent among them are:

- **Spalart-Allmaras:** A one-equation model that approximates turbulent viscosity, in conjunction with the Navier-Stokes equations. It is well-suited for aerospace applications involving wall-adhering flows, such as those over wings and aerofoils. The model

effectively predicts flows with adverse pressure gradient, while producing large errors when applied to free-shear flows. [37]

- **K-epsilon ($k-\varepsilon$):** A two-equation model that derives transport equations for turbulence kinetic energy (k) and the dissipation rate of turbulence kinetic energy (ε). It excels in predicting mixing length and algebraical prescription of turbulent length scales in flows of moderate to high complexity. It is well-suited for free-shear flows but tends to produce significant errors in cases with strong adverse pressure gradients. [38]
- **K-omega ($k-\omega$):** Another two-equation model, that derives transport equations for turbulence kinetic energy (k) and specific dissipation rate (ω). While similar to $k-\varepsilon$, it is more accurate in solving boundary layers with adverse pressure gradients. However, it is sensitive to free-stream boundary conditions in external flows. [39]
- **K-omega Shear-Stress Transport (SST $k-\omega$):** A hybrid model combining the strengths of the two previous models. K-omega equations are applied to solve the near-wall region, typically capturing the viscous sub-layer, switching to $k-\varepsilon$ in the free-stream region. By using both approaches complementary, SST negates their most limiting shortcomings. Despite its improved versatility, it may over-predict turbulence levels in regions with a significant velocity gradient. [40]

3.6 State-of-the-Art

Several scientific articles closely related to the subject of bobsleigh aerodynamics were identified, the findings of which were carefully considered and integrated into the present analysis.

It is noteworthy that all of these studies employed three-dimensional RANS turbulence models, notably SST $k-\omega$, Standard $k-\varepsilon$ and Realizable $k-\varepsilon$.

As previously mentioned in Chapter 3.1, the IBSF imposes strict regulations on bobsleigh shape to ensure athlete safety and prevent unfair aerodynamic advantages. However, the design of bumpers is subject to less rigid constraints, requiring adherence to only general size and shape limitations.

Shim et al. [4] capitalized on this relative freedom to optimize the front and rear bumper shapes with the goal of minimizing aerodynamic drag. Through a parametric study, the researchers identified the following design parameters as having the most significant influence on aerodynamic drag generation (Figure 3.9):

- Ratio of thickness of front bumper to the bobsleigh width $\left(\frac{T}{W}\right)$
- Ratio of the major axis length of front bumper to the bobsleigh width $\left(\frac{L_f}{W}\right)$
- Ratio of the front radius of the cowling to bobsleigh length $\left(\frac{R_f}{L}\right)$

- Ratio of the side radius of the cowling to bobsleigh length $\left(\frac{R_S}{L}\right)$

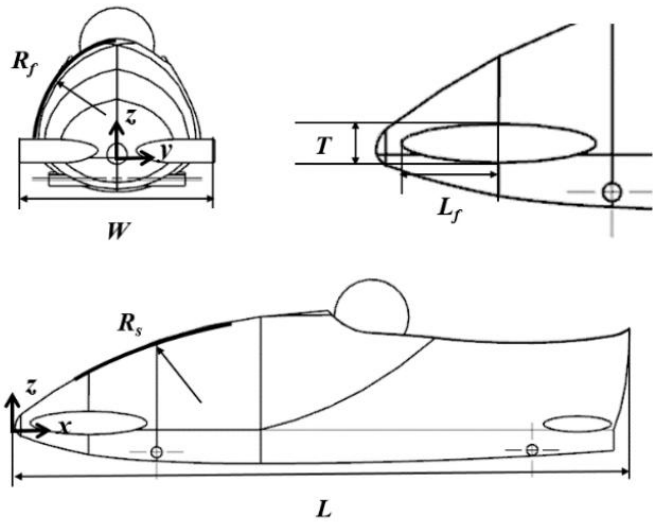

Figure 3.9: Visual representation of geometric parameters [4]

The optimal parameters were observed to be $\frac{T}{W} = 0.14$, $\frac{R_S}{L} = 1.0$, $\frac{R_f}{L} = 0.16$ and $\frac{L_f}{W} = 0.30$.

The same team reports then, through a consequent study [2], additional significant design parameters (Figure 3.10):

- Leading angle of the front bumper (θ_1)
- Ratio of the distance between the front bumper and the ground to the thickness of the front bumper $\left(\frac{H_1}{T}\right)$
- Ratio of the distance between the rear bumper and the ground to the thickness of the front bumper $\left(\frac{H_2}{T}\right)$

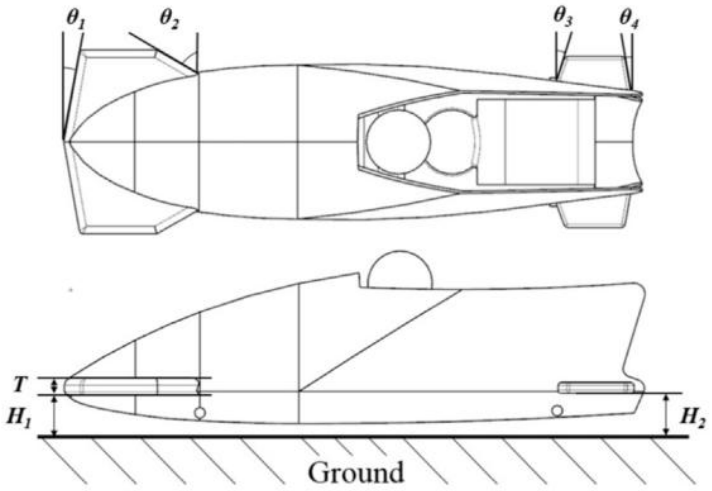

Figure 3.10: Additional geometric parameters [2]

Based on these three variables, a discrete design space consisting of 25 points was generated to represent a wide range of potential designs. The analysis revealed that a lower drag coefficient could be achieved by reducing the distance between the front bumper and the ground and increasing the leading angle of the front bumper, compared to the reference shape. This optimization resulted in a reduction in aerodynamic drag of 3.08% with the optimal design variables being $\theta_1 = 19.988°$, $\frac{H_1}{T} = 1.701$ and $\frac{H_2}{T} = 2.399$.

Winkler and Pernpeintner [41] conducted a comprehensive CFD analysis of over 100 bobsleigh shapes, applying the results to a preliminary design process. The flow domain was discretized using a mesh composed of triangular and tetrahedral elements, ensuring high mesh quality and accurate representation of the bobsleigh's geometry.

Two distinct testing domains were created, recreating the varying conditions found in the descent through the ice track:

- A straight section, where the lateral walls of the track are in close proximity to the sleigh, significantly influencing flow development.
- A curve section, where no confining walls are immediately adjacent to the sleigh, allowing for less constrained flow development. It is important to note that both the inlet flow angle and the sleigh's yaw angle were maintained constant throughout these simulations, with only the wall configuration being altered.

A single inlet flow velocity (36.11 m/s, representing an average speed during the late stages of a run) was considered. The floor was modelled as both stationary, simulating wind tunnel conditions, and as a moving surface (with the same velocity) to account for the relative motion between the bobsleigh and the track.

In all scenarios, pressure drag accounted for approximately 80% of the total drag. The presence of walls in the straight section resulted in a 4% increase in drag for a stationary floor and a 5% increase for a moving floor. Conversely, a 1% decrease in drag was observed for the moving floor condition, suggesting that wind tunnel tests may slightly overestimate drag compared to actual race conditions.

The study sought to minimize the drag contribution of individual components, with the cowling and front axle demonstrating the most significant improvements. The cowling's enhanced performance was primarily attributed to overall shape modifications, while the rear axle's shape remained relatively unchanged but benefited from additional coverage provided by the cowling. Finally, simulations confirmed the substantial influence of the brakeman's posture on aerodynamic drag. A forward lean at the right angle by the brakeman could effectively minimize negative pressure and reduce drag.

Following the CFD analysis, wind tunnel testing was conducted on a 1:3 scale model. This approach allowed for the evaluation of minor design changes in a more time-efficient manner compared to CFD simulations. Additionally, wind tunnel tests were used to validate the CFD results.

Key findings from the wind tunnel experiments included a 4% underestimation of drag by the CFD simulations and a decrease in drag with increasing forward lean of the brakeman. A more detailed analysis of the optimal brakeman position is provided in a subsequent section.

The geometry of the diffuser (Figure 3.11) was also empirically studied, revealing that an apex angle of 2°/4.5° (slim diffuser contour) or 6.7° (bulky diffuser contour) resulted in the least drag generation.

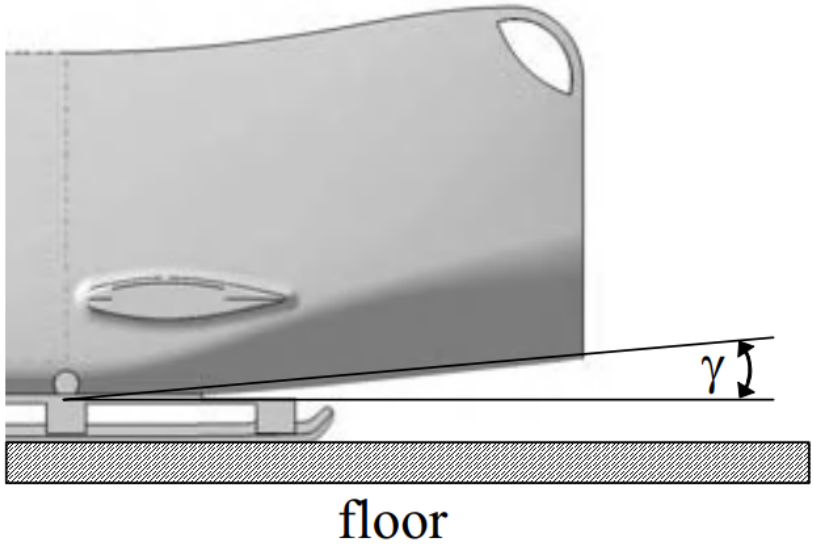

Figure 3.11: Angle of the diffuser [41]

Chowdhury et al. [6] manufactured a 1:2 scale model of a standard 2-men bobsleigh for wind tunnel testing. Wool tufts were mounted on the surfaces in direct contact with the flow stream, which through changes in vibration show variations in flow behaviour. The studied airspeeds ranged from 40 to 120 km/h.

The data showed a significant decrease in drag at 55° brakeman body angle for speeds over 80 km/h. Further inclination of the athlete substantially increased drag, until 35°, from where drag would decrease once more (Figure 3.12).

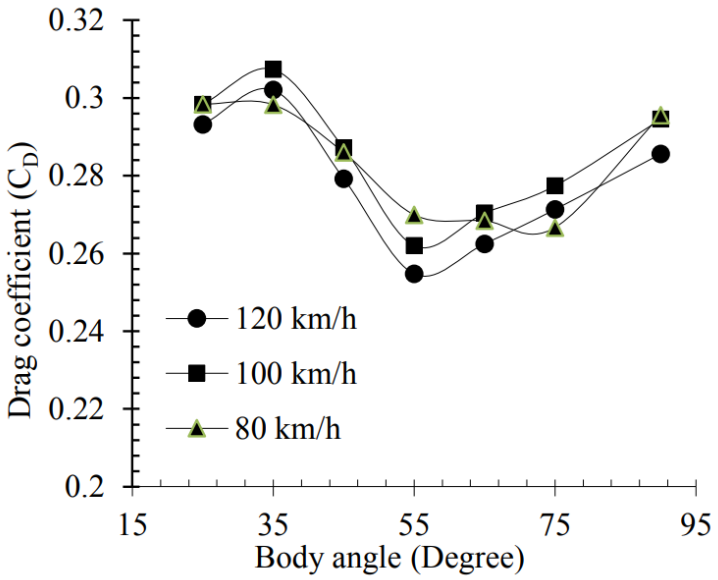

Figure 3.12: Influence of brakeman's angle on drag coefficient [6]

Evidently, this contradicts the findings of Winkler and Pernpeintner [41] and its subsequent study [42], where drag would constantly decrease with the brakeman's inclination.

Gibertini et al. [3] reported that increasing the height of the bobsleigh underside from the standard 50 *mm* to 70 *mm* reduces drag generation by taking advantage of ground effects.

Motallebi et al. [5] propose two further approaches to improve performance: a sharp nose and flared sidewalls.

The nose shape, though having a limited effect on pressure drag of the cowling, significantly influences airflow development over the entire bobsleigh [25]. The researchers employed a sharp nose design to energise boundary layer flow along the mid-section of the nose, allowing it to resist a higher adverse pressure gradient when colliding with the driver's head. This effect reduces the size of the wake separation between the nose surface and the driver's head. Additionally, the sharp nose would also energise the flow in the side parts of the nose, accelerating the flow around the crew, also reducing the separated region behind them. Figure 3.13 shows a comparison between a "shark-nose" and a traditional smoother nose contour.

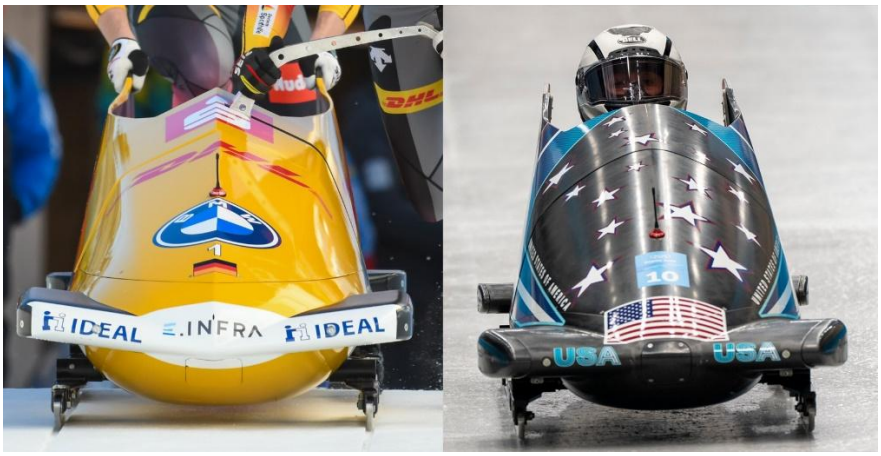

Figure 3.13: Comparison of sharper (left) and smoother (right) nose contours [43] [44]

Flared sidewalls further widen the rear of the bobsleigh to gradually accelerate the flow, encouraging adhesion to the surface. This design encourages it to continue on the flanks for longer, before being sucked by the pressure gradient in the cavity, where significant streamline mixing and strong vortices occur.

Both modifications were tested using a quarter-scale model in a wind tunnel. Results indicated a reduction in drag for both modifications, for Reynolds numbers below 280 000, increasing for higher Reynolds numbers, when compared to the reference model. This effect could be beneficial, as the modified versions would produce higher accelerations in the early stages of the race, potentially establishing an initial lead even if drag increases at higher speeds.

Chapter 4

4 Methodology

This chapter provides a detailed description of the methodology employed in this work. It serves to validate good scientific practice and ensure this work can be reproduced by tracing the steps discussed in this section.

4.1 Hardware

Meshing and CFD operations were performed on a desktop workstation provided by UBI. The workstation was remotely accessed by the author using the *Windows Remote Desktop Connection* tool, enabling continuous monitoring and adjustment of simulation processes.

The hardware specifications of the used workstation are shown in Table 4.1.

Table 4.1: Remote workstation hardware specifications

CPU	$\mathbf{12th\ Intel\ Core\ i7-12700}\ (\mathbf{2.10\ GHz;\ 12\ cores})$
GPU	$NVIDIA\ T400\ 4GB$
Memory	$16.0\ GB$

4.2 Computer-Aided Design (CAD)

The computer-aided design process was done using two distinct software programmes. The initial phase of design was entirely done in Solidworks 2023 Student Edition, after which the CAD files were exported to ANSYS SpaceClaim for further processing in preparation for meshing.

4.2.1 Solidworks

The initial bobsleigh model, hereafter referred to as the *Reference Model*, was developed using top, front and side projections of high-performance designs as references. These reference images, obtained through internet searches, included photographs taken in competitions and technical drawings of bobsleighs. To ensure the design complied with IBSF official guidelines, the IBSF Rule Book [22] was consulted to verify dimensions and geometric constraints.

To facilitate the meshing process, some simplifications were applied, making the CAD model differ from a detailed representation of a real bobsleigh. The main simplifications were:

- **Omission of runners and axles**, as the aerodynamic influence of their protruding bodies was beyond the scope of this study.
- **Exclusion of push handles and cowling dividing line**, since these components are either retracted during a run or have little aerodynamic impact
- **Fixed front and rear cowlings**, given that the effects of steering were not considered in this study.
- **Non-hollow cowling,** as the cowling component in front of the driver's body is considered solid, no internal flow effects were considered in this area.
- **Idealised representation of athletes**, with their bodies modelled as simplified geometric shapes. The brakeman's back ends in a 45° slant, corresponding to the optimal posture discussed in Chapter 3.6.

The geometry used in the initial simulations is shown in Figure 4.1 and Figure 4.2.

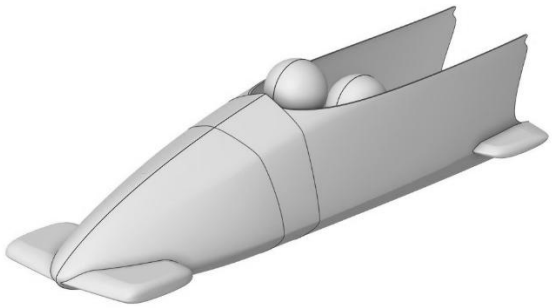

Figure 4.1: CAD geometry of the Reference Model

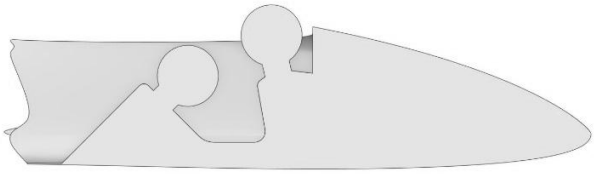

Figure 4.2: Side view of the CAD geometry on the symmetry plane

To ensure compatibility with external CAD software, it was exported in STEP format, an interoperable file format which facilitates the exchange of geometric data between different CAD platforms.

4.2.2 ANSYS SpaceClaim

Upon import into ANSYS SpaceClaim, the model was analysed for geometrical errors, a standard procedure for imported geometry. All detected errors, including non-critical ones, were repaired to prevent additional difficulties in the meshing process.

A fluid domain control volume was generated by creating a shell-like solid structure with an internal void matching the topology of the imported model. The control volume defines the computational fluid domain which will be meshed for simulation.

As all simulated cases involve an airflow parallel to the bobsleigh's longitudinal axis, the fluid domain can be split along the bobsleigh symmetry plane, allowing only one half of the bobsleigh to be modelled in the simulations. This approach assumes the resulting airflow is symmetrical in both sides, meaning the results on the non-simulated side are considered identical. This method can be used to reduce computational cost without sacrificing accuracy.

The control volume dimensions were selected to ensure that the relevant development of the flow around the bobsleigh geometry is fully captured while minimising its computational cost by limiting the required number of mesh cells. Preliminary analysis allowed to determine appropriate dimensions, finding a good balance between accuracy and efficiency.

Additionally, frontal blockage ratio was evaluated:

$$B = \frac{A}{A_e} = \frac{0.1928\ m^2}{5.59\ m^2} = 3.45\% \tag{4.1}$$

where A_e is the control volume cross sectional area.

A high blockage ratio might introduce unrealistic flow behaviour, such as increased pressure and drag generation, which would not occur in open-air conditions. If blockage effects are too high, the accuracy of aerodynamic forces and wake structures will be reduced. However, the calculated ratio is within acceptable limits, as blockage effects can usually be neglected for ratio values below 10%, meaning the control volume dimensions will have a very low impact on results. [45]

Figure 4.3 shows the control volume, detailing its dimensions and boundary terminology. Boundary terminology is used to specify meshing commands in the meshing software and to set boundary conditions in the solution setup. Boundary conditions are further discussed in Chapter 4.5.3.

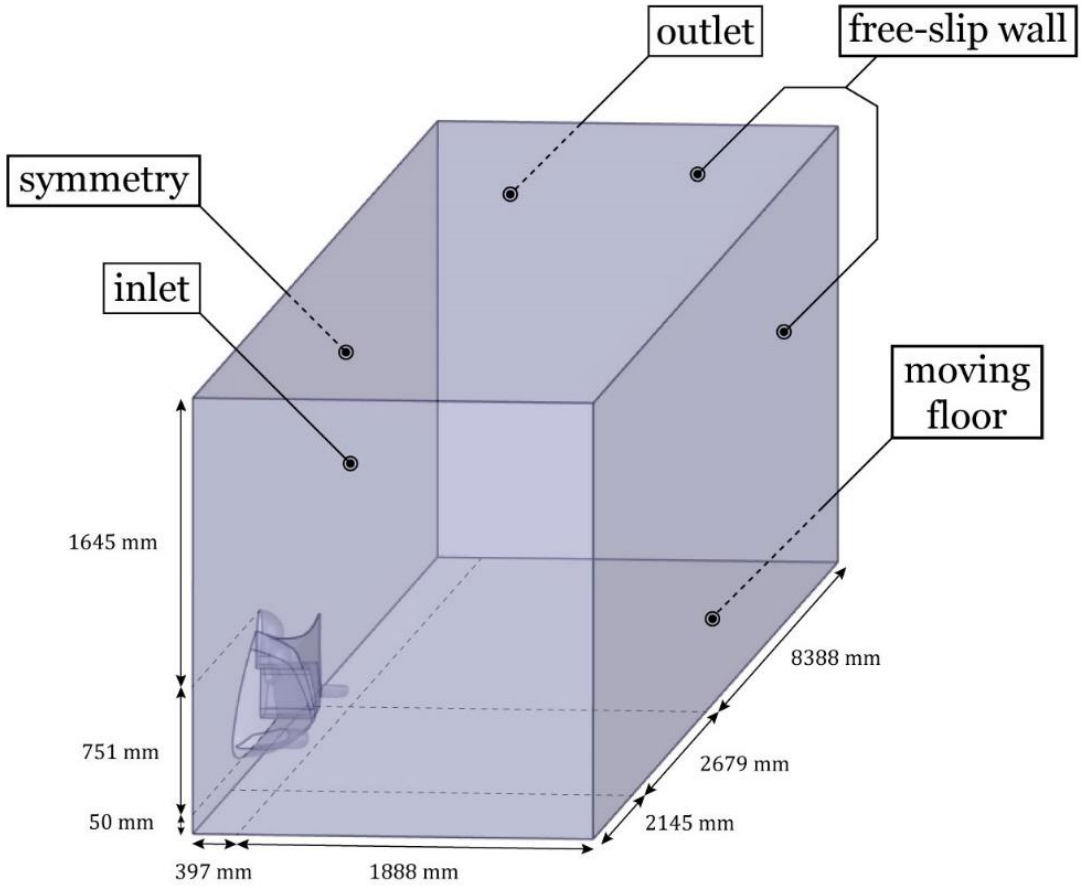

Figure 4.3: Control volume dimensions and boundary terminology

4.3 Enhanced Model

After extensive experimentation and iterative refinement aimed at reducing aerodynamic drag, the *Enhanced Model* was developed. Since the *Reference Model* already closely followed the geometric principles of high-performance bobsleigh designs, effective improvements came from small-scale modifications, guided by a careful analysis of flow behaviour. Several improvement features from existing research were applied with varying degrees of success.

Figure 4.4 compares the geometric features of both models, highlighting the most relevant dimensions, providing a better understanding of the applied modifications.

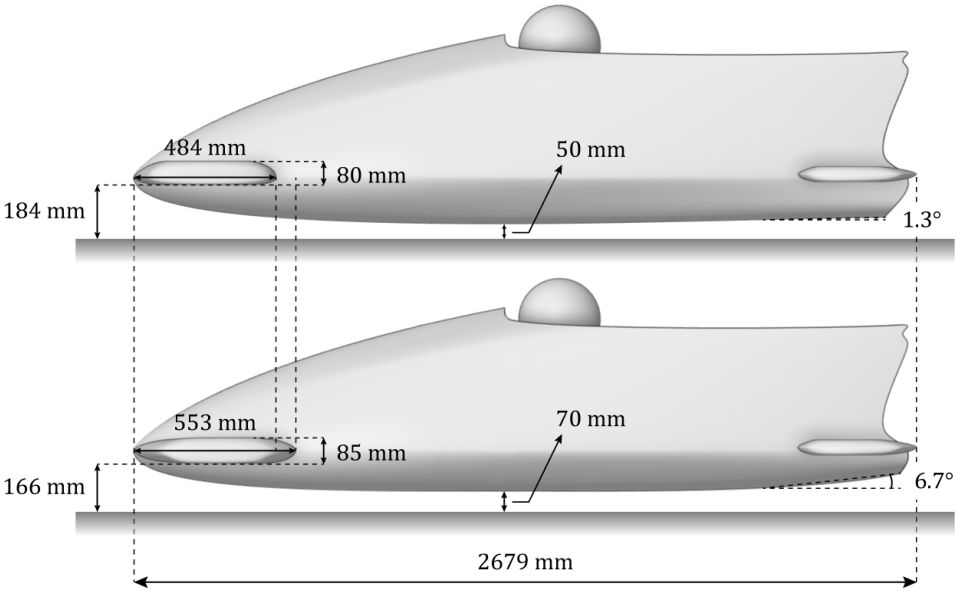

Figure 4.4: Side-view comparison of the geometries of the Reference Model (top) and the Enhanced Model (bottom)

4.3.1 Underside Flow Ground Effects

The flow in the region between the bobsleigh underside and the ground is reported in [25] to exhibit a Venturi effect, which can be described by the Continuity Equation, presented in Equation (3.13). For a steady incompressible one-dimensional flow, it can be expressed as [46]:

$$A_i V_i = A_o V_o \tag{4.2}$$

where A_i is the control volume inlet cross-sectional area, V_i is the control volume inlet flow velocity, A_o is the control volume outlet cross-sectional area and V_o is the control volume outlet flow velocity.

Increasing the height of this control volume (the clearance between the bobsleigh underside and the ground), reduces flow velocity, leading to a more uniform pressure distribution in the region, which has the potential to reduce aerodynamic drag. For this reason, the underside of the cowling was raised by 20 *mm*, increasing the clearance to 70 *mm*, a value identified in [3] as preferable for minimising drag.

Additionally, the *Enhanced Model* applies a diffuser to decelerate the flow ejected in the bottom rear end of the cowling, reducing adverse pressure gradients and reducing drag. The applied diffuser geometry is consistent with the findings from [41], which indicate that a diffuser with a bulky contour with an apex angle of 6.7° is optimal in similar conditions.

4.3.2 Front Bumper Modifications

The enhanced bumper geometry was lengthened by 14.35%, thickening its tail section to 85 *mm*, tapering to the minimum thickness limit, 80 *mm*, at the front. A lengthier and tapered bumper proved to be beneficial, enabling the leading edge of the bumper to be more slender, improving flow attachment along the surface and delaying its separation, as observed in [4].

Furthermore, the front bumper height was lowered by 18 *mm* relative to the Reference Model. This adjustment aimed to reduce the size of the low-velocity region after the bumper and redirect the stagnation region closer to the rear bumper, minimising disturbances to the free-stream. [2]

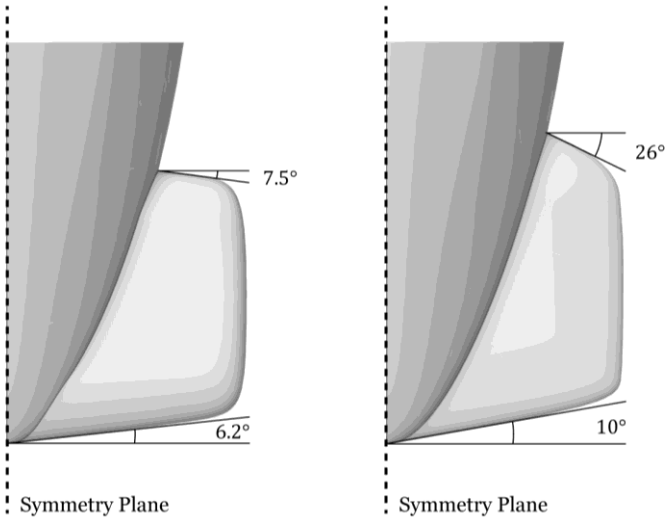

Figure 4.5: Top-view comparison of the geometries of the Reference Model (left) and the Enhanced Model (right)

The front bumper leading and trailing edges centred in height and their sweep angles were increased, intending to delay flow separation and reduce the size of the resulting turbulent wake, as referenced in [2] (Figure 4.5). Although this article remarks gains in performance for a leading sweep angle as high as 20°, this configuration was not optimal in the present study, as it increased flow separation at the leading edge. This inconsistency is likely due to differences in used bumper geometries: while the referenced article utilised simplified bumper models, suitable for a streamlined parametric study, the present report employed competition-accurate bumper shapes.

Although, the front bumper geometry changes applied in the *Enhanced Model* inevitably increase skin friction drag due to the larger surface area exposed to the airflow, they make the flow around the bumper more streamlined, counteracting the additional frictional losses.

4.3.3 Limited-Impact Adjustments

Consistent with the findings from prior research, changes in rear bumper geometry, bumper angle of attack or overall bobsleigh length did not produce significant reductions in drag generation. This further highlights the influence of adjustments in the underside of the bobsleigh and in front bumper geometry in improving aerodynamic performance.

4.4 Meshing

ANSYS Workbench offers two distinct meshing modules which are among the most used meshing tools for CFD, ANSYS Meshing and Fluent Meshing. While both are capable of generating suitable meshes for most cases, their approaches and functionalities differ significantly, leading to different results. Therefore, it is essential to evaluate the characteristics of each module to determine the most appropriate choice.

The key differences between them are as follows:

- **Scope:** ANSYS Meshing is a general-purpose meshing tool, employed in multiple applications such as CFD, Electromagnetics and Structural Finite Elements Analysis. On the other hand, Fluent Meshing is specifically tailored for CFD applications, containing several features optimised for ANSYS Fluent.
- **Features:** The workflows of both modules reflect their contrasting scopes. ANSYS Meshing provides a greater flexibility and higher level of user control, being well-suited for generating highly customised meshes. Fluent Meshing excels in automatic mesh refinement and optimization, allowing for a more streamlined meshing process.
- **Volume mesh generation:** While ANSYS Meshing primarily generates structured meshes composed of hexahedral and tetrahedral cells, Fluent Meshing introduces polyhedral cells, which improve greatly computational efficiency without sacrificing geometry fidelity and cell quality (Figure 4.6). [47]

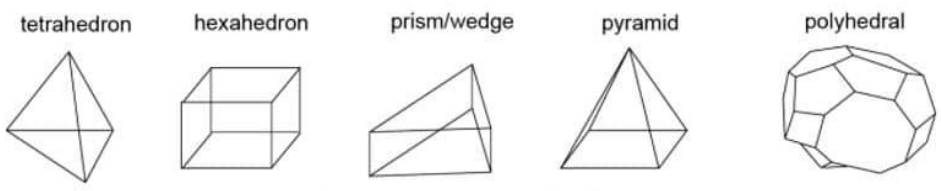

Figure 4.6: 3D Element Types [48]

Fluent Meshing was the chosen module for this study, mainly due to its integration with ANSYS Fluent and the availability of the Poly-Hexcore meshing method, which was employed in this project. This approach combines polyhedral cells in near-surface regions with hexahedral cells in the free flow (Figure 4.7). The Poly-Hexcore method is widely utilized in CFD due to its ability to further reduce the total cell count compared to a fully polyhedral mesh.

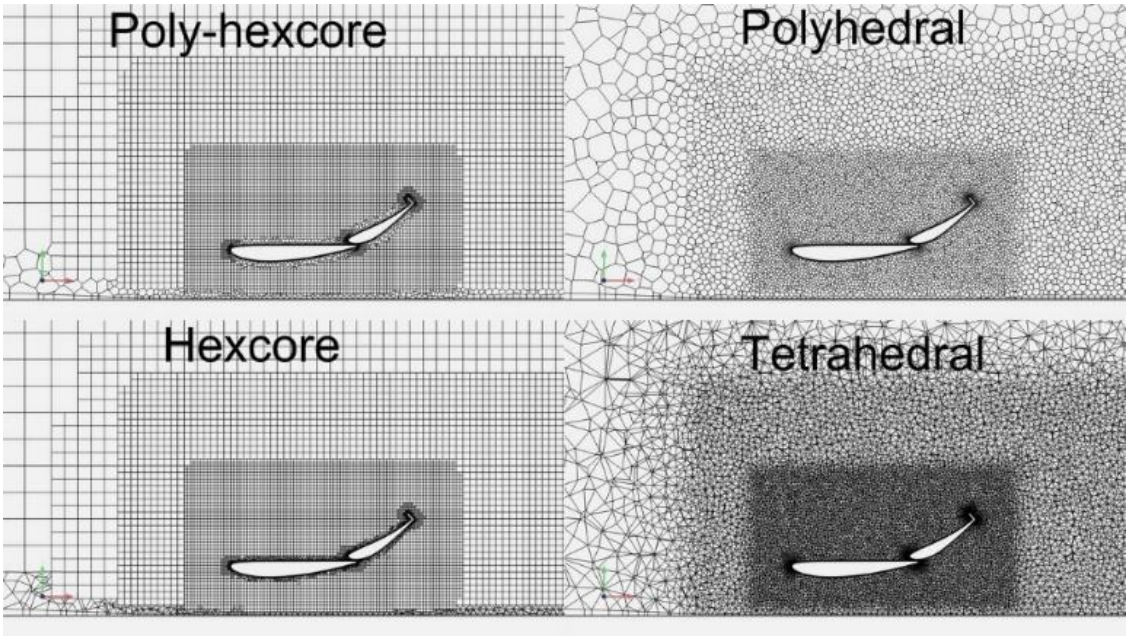

Figure 4.7: Volume mesh methods in Fluent Meshing [49]

To ensure good numerical solutions, all generated meshes respected several cell quality criteria, found in Table 4.2. Fluent Meshing's diagnostic and automatic mesh improvement tools were of great help in refining mesh quality. In cases where all corrections were insufficient to improve all cells, the final mesh was reviewed to confirm they would not affect the solution, if present in a small quantity.

Table 4.2: Cell quality parameters

Skewness (surface mesh)	Orthogonality	Aspect ratio
<0.65	>0.15	<1000

4.4.1 Local Refinement Regions

Local refinement of the mesh is essential in flow regions with high complexity, particularly near the bobsleigh surface and in the wake region, to accurately capture all aerodynamic phenomena. The adopted method for this study is *Local Refinement Regions*, a functionality available in

Fluent Meshing. This tool analyses the object geometry and generates a refined mesh zone around it. Additionally, it extends a wake refinement region downstream, where the cell size is twice that of the near-wall refinement region. This ensures that relevant flow structures are adequately resolved, as illustrated in Figure 4.8.

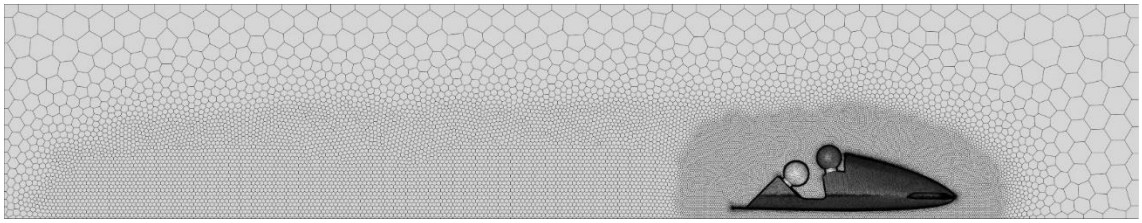

Figure 4.8: Side view of the meshed fluid domain at the symmetry plane

An alternative approach is the Bodies of Influence method, where specific predefined volumes, designed in the CAD phase, delineate refinement zones. However, preliminary testing indicated Local Refinement Regions provided a greater efficiency coupled with added flexibility.

4.4.2 Inflation Layers

The presence of solid walls significantly affects airflow due to the formation of viscosity-prevalent regions, known as the boundary layer, which greatly influence solution variables, as discussed in Chapter 3.4. Inflation layers are a commonly used method in meshing to accurately capture the development of the boundary layer.

However, there are two main approaches for their application in the mesh:

Resolving the boundary layer: implementing inflation layers fine enough to directly solve the velocity gradients down to the wall. For this method, the first layer must be placed in the viscous sub-layer (preferably $y^+ \approx 1$). This approach is the most accurate but requires the most computational resources.

Using wall functions: these functions calculate the near-wall gradients using the Law of the Wall equations. For this method, the first cell must be placed in the log-law region ($y^+ > 30$) to guarantee accurate predictions. This method significantly reduces computational cost as it requires fewer mesh cells in the boundary layer region. [50]

As the chosen turbulence closing model was a $k - \varepsilon$ model, wall functions were the most adequate choice for the intended simulations. They model the flow in near-wall regions, where $k - \varepsilon$ has reduced accuracy, bridging them with the free-stream, where the model produces correct predictions.

The implementation of inflation layers in this study is shown in Figure 4.9. The Poly-Hexcore progression from prismatic inflation layer cells to transition polyhedral cells, and finally to the hexahedral cells in the fully developed flow region, can be observed.

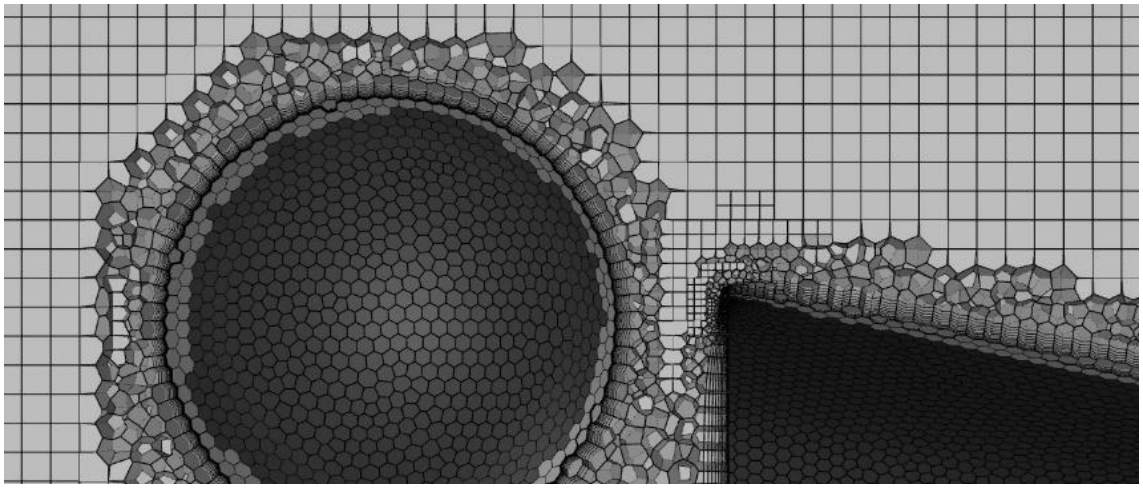

Figure 4.9: Close-up of mesh on the driver's helmet region

4.5 Solution Setup

After generating a satisfactory mesh, it is imported to ANSYS Fluent, the CFD solver used for this study. The solution setup in Fluent is a critical step, as it defines all simulation conditions and numerical methods used in the analysis.

4.5.1 Turbulence Model

For turbulence modelling, **Realizable $k-\varepsilon$** was selected. This model differs from others in the $k-\varepsilon$ family through alternative formulations for turbulent viscosity and dissipation rate, enhancing its predictions. In particular, it provides better accuracy in flows with considerable streamline curvature, vortices, and rotational effects, making it a suitable choice for the present study. The near-wall region is modelled using **Non-Equilibrium Wall Functions**. This method offers advantages over Standard Wall Functions by accounting for strong pressure gradients and rapid changes in mean flow and turbulence, which are relevant in cases involving flow separation, reattachment, and impingement. [51]

Alternative models, such as SST $k-\omega$, would certainly provide more accurate results, particularly in directly resolving boundary layer effects. Preliminary testing determined this approach could not be applied due to processing constraints and the required mesh refinement for capturing flow phenomena around the bobsleigh geometry.

4.5.2 Reference Values

Reference values are essential for calculating force coefficients, which serve as indicators for monitoring and validating the solution. The inserted reference values are presented in Table 4.3.

Table 4.3: Fluent reference values

$\rho\ [kg/m^3]$	$L\ [m]$	$\mu\ [kg/(m\ s)]$	$p\ [Pa]$	$T\ [K]$
1.225	2.679	1.7894×10^{-5}	101325	288.16

The reference length used is the total length of the bobsleigh, consistent among both the *Reference Model* and the *Enhanced Model*. Frontal area values are dependent on model geometry and are specified in Chapter 5.3.

4.5.3 Boundary Conditions

Boundary conditions define flow properties and conditions for the interaction between the domain boundaries and the flow. The inputted boundary conditions can be found in Appendix A.

4.5.4 Discretisation Methods

Discretisation methods influence the solution convergence, stability and accuracy. The selected discretisation methods are laid out in Table 4.4.

Table 4.4: Discretisation Methods

Pressure-Based Solution Method	Coupled
Gradient Discretization	Least Squares Cell Based
Pressure Discretization	Second Order
Momentum Discretization	Second Order Upwind
Turbulent Kinetic Energy Discretization	Second Order Upwind
Turbulent Dissipation Rate Discretization	Second Order Upwind

Pressure-Velocity coupling enables the simultaneous solving of momentum and pressure-based continuity equations, obtaining a more efficient and robust convergence in steady-state flows. Second-Order accuracy in spatial discretisation allows for higher result accuracy and reduced numerical diffusion, when compared to first-order interpolation schemes.

4.5.5 Solution Initialisation

Before the main simulation, each case went through a hybrid initialisation process, followed by a Full Multigrid (FMG) Initialisation. This method solves the flow on the coarsest levels of the domain, improving the initial solution in a nearly computationally inexpensive manner. Preliminary testing confirmed all bobsleigh flow problems benefitted from FMG initialisation.

4.5.6 Report Values and Solution Convergence

Report values were used as monitors on solution convergence and stability, along with residual values of the variables in the turbulence closing model. The following report values were tracked:

- Drag coefficient
- Lift coefficient
- Pitching moment coefficient

The point used for calculating the pitching moment coefficient was assumed to be located at the centre of mass, placed approximately near the driver's back. This assumption might not be completely accurate, but further calculations on this matter were deemed unnecessary for the objectives of this study, as the primary focus was on aerodynamic forces rather than precise moment calculations.

The simulations were terminated once residual and report values were stabilised, having produced sufficient data for statistical averaging of results.

4.6 Mesh Independence and Validation

A mesh independence study was conducted to find the most adequate balance between numerical accuracy and computational efficiency. The mesh was progressively refined until further refinement produced negligible changes on the monitored coefficients. Changes below 2.5% in each value between successive mesh refinements was considered unnecessary.

The final, most efficient mesh is defined by the parameters presented in

Table 4.5.

Table 4.5: Final mesh parameters

Minimum cell size [$\boldsymbol{mm}$]	**1**
Maximum cell size [$\boldsymbol{mm}$]	10
Cell growth rate	1.2
Curvature normal angle [°]	12
Local refinement region cell size [$\boldsymbol{mm}$]	12
Quantity of inflation layers	10
Inflation layer transition ratio	0.272

These parameters remained consistent across all simulations for both studied airflow velocities: 15 m/s and 35 m/s.

Figure 4.10 presents the mesh convergence study for the simulations conducted in this work, using the control volume shown in Figure 4.3. All reported results were obtained from meshes consisting of approximately 2,200,000 cells, corresponding to the second marker in the chart. This mesh configuration shows a relative error of 1.24% compared with the third marker, while significantly reducing cell count, thereby greatly reducing simulation run time.

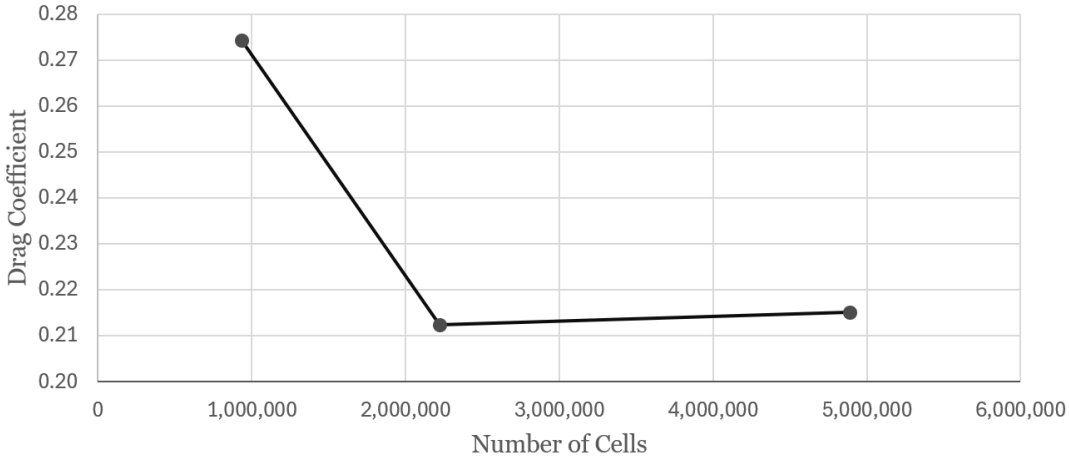

Figure 4.10: Mesh convergence study for the conducted simulations

4.6.1 Near-Wall Treatment

Particular attention was given to near-wall resolution. A value of y^+ of approximately 32.5 was targeted for all relevant surfaces, ensuring they would be well within the log-law layer of the

turbulent boundary layer. Figure 4.11 illustrates the distribution of y^+ values along the bobsleigh's longitudinal axis, where the reference point is positioned at the assumed centre of mass, located approximately at the driver's back.

The results indicate that not all surfaces achieved a valid y^+ of over 30. This was not corrected as forcing inflation layers to maintain a value of $y^+ > 30$ would have resulted in excessively thick layers, which could compromise the fidelity of boundary layer predictions. So, a balance was found, where the majority of relevant surfaces were applied a $y^+ > 30$ without compromising the fidelity of boundary layer predictions.

The first layer height values used in the simulations were:

- For 35 m/s cases: 0.728 mm to 1.09 mm
- For 15 m/s cases: 1.59 mm to 1.92 mm

In addition to y^+ monitoring, boundary layer resolution was analysed through the quantity of inflation layers and transition ratio between them, evaluating its impact on results. The used values (shown in

Table 4.5) were deemed adequate, permitting the relevant capturing of the velocity gradient within the boundary layer.

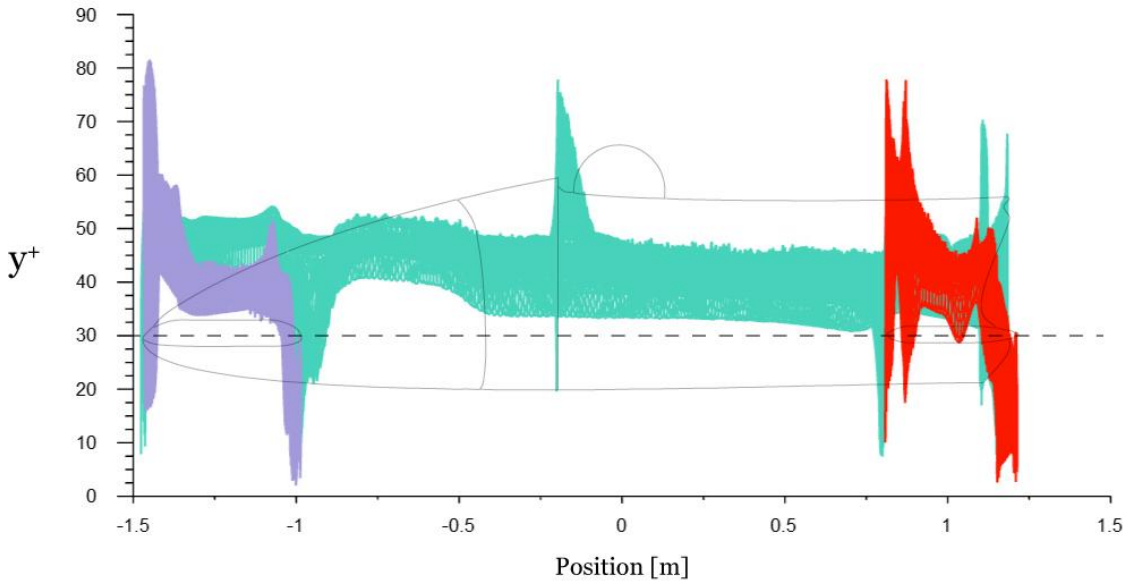

Figure 4.11: y^+ distribution (Reference Model, 35 m/s) along the bobsleigh longitudinal axis in the cowling outer wall (cyan), front bumper (purple) and rear bumper (red) surfaces

Chapter 5

5 Results and Discussion

This chapter presents the results obtained from CFD simulations on bobsleigh aerodynamics. The analysis focuses on flow phenomena and aerodynamic forces across several scenarios such as at the speeds of 35 m/s (representing the typical velocity at the fastest portions of the track) and 15 m/s (representing push start conditions). Additionally, the study examines flow behaviour in straight track with confining walls investigating the aerodynamic effects induced by track geometry.

5.1 Flow Phenomena (15 m/s)

The simulations conducted at a free-stream velocity of 15 m/s, representing a velocity reached during the final stages of the push start showed overall flow structures, including separation and vortex-generating regions, remain similar to those observed at 35 m/s, with the magnitudes of aerodynamic forces, vortex intensity, and overall flow velocity being substantially lower.

Additionally, the reduction of Reynolds number leads to the formation of thicker boundary layers, which was accounted for in the meshing process by applying thicker inflation layers. This effect makes the velocity transition from the wall to the free-stream is more gradual, reducing wall shear stress and consequently leading to lower skin friction drag.

Given the flow structure similarities with the results from 35 m/s analysis, 15 m/s results were deemed not to be as relevant for the study. Subsequent chapters will only discuss results for 35 m/s runs.

5.2 Flow Phenomena (35 m/s)

This chapter analyses flow phenomena observed in the CFD simulations at a free stream velocity of 35 m/s. The aerodynamic structures in the Reference Model and Enhanced Model are compared where relevant to highlight the effects of the modifications.

The incoming flow initially interacts with the nose and the leading edge of the front bumpers, resulting in a high-pressure region caused by flow stagnation. The air then accelerates smoothly over the nose, front bumper, side walls and underside.

Figure 5.1 highlights the most influential vortex generation regions, particularly the bumpers, cavity leading section, athletes' helmets, side walls and the underside. These regions will be further discussed in the following sub-chapters.

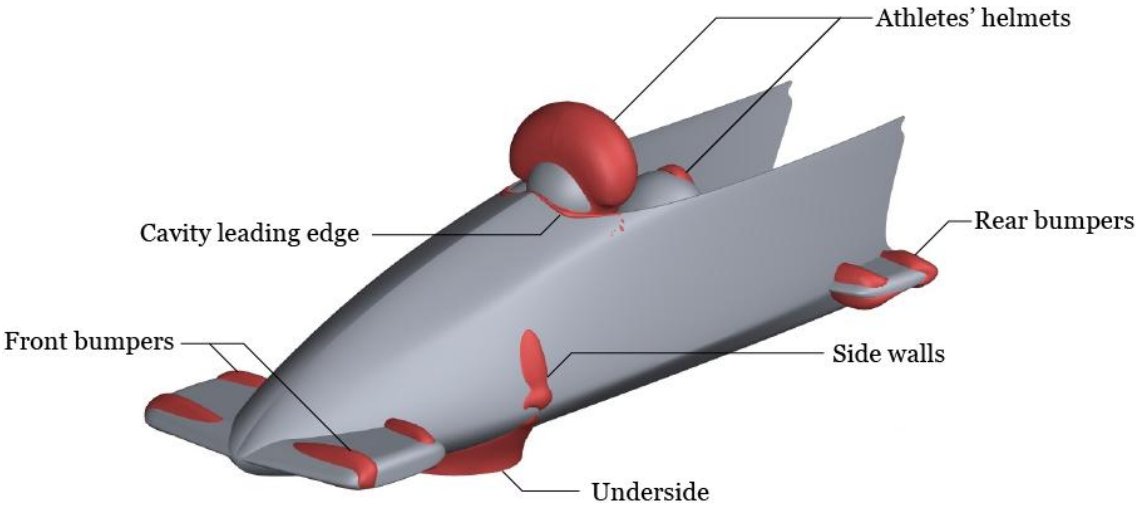

Figure 5.1: Iso-surface of Static Pressure = −200 Pa on the Reference Model

5.2.1 Cavity Region

The cavity is a primary source of drag, along with the driver's helmet, which should be shielded from the free-stream as effectively as possible.

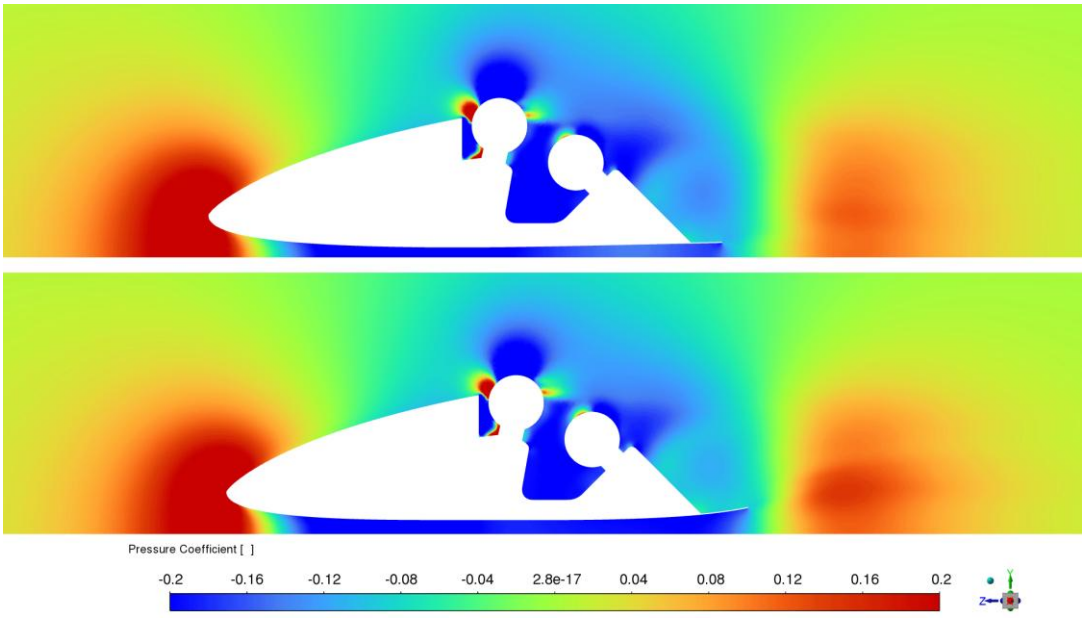

Figure 5.2: Pressure coefficient contour on the symmetry plane for the Reference Model (top) and the Enhanced Model (bottom)

As illustrated in Figure 5.2, airflow over the nose enters the cavity region and collides with the helmets of the crew members, leading to stagnation zones in the front-facing areas of both athletes. Afterwards, the flow over the helmets experiences strong acceleration, drastically reducing pressure in the region, indicative of flow separation. The entirety of the cavity is subject to significant vorticity, generated by the vortices shed from the driver's helmet and the suction of external flow into the cavity.

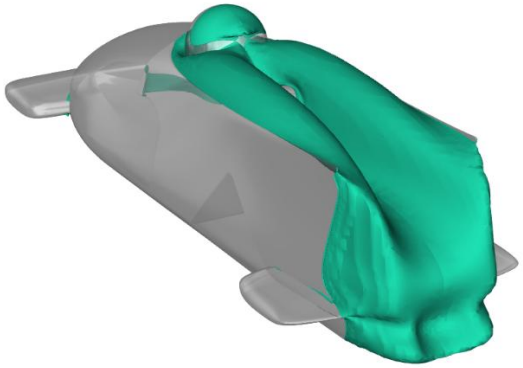

Figure 5.3: Iso-surface of zero total pressure on the Reference Model

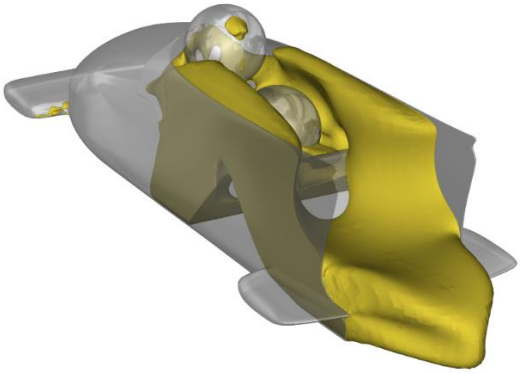

Figure 5.4: Iso-surface of Z-velocity = 0.1 m/s on the Reference Model

Figure 5.3 depicts the wake induced by the leading section of the cavity and the driver's helmet. Two distinct vortices are visible behind the helmet. However, as noted in [25], the accuracy of these results may be influenced by the use of a symmetry plane in the simulation. The symmetry boundary condition could introduce artificial limitations affecting vortex structures.

Figure 5.4 shows recirculation phenomena, namely occurring in the back of the driver's helmet, cavity interior walls and in the bottom rear section of the bobsleigh. Figure 5.5 further illustrates flow circulation in particles entering the cavity through the nose. The central flow structures bypass the driver's helmet but suffer intense recirculation around the brakeman's back. Additionally, air attached to the side walls is sucked into the cavity, generating vortices which further contribute to aerodynamic drag.

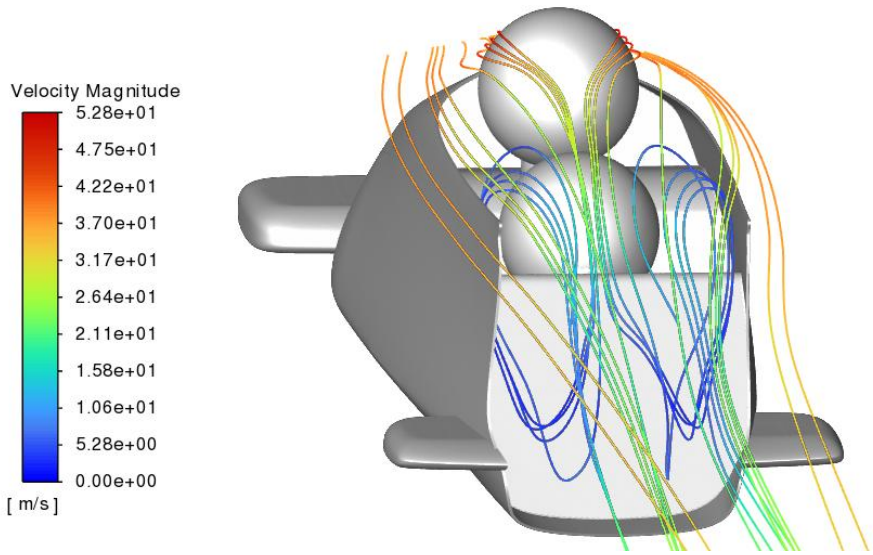

Figure 5.5: Flow streamlines and velocity magnitude within the cavity in the Reference Model

5.2.2 Underside Flow

As discussed in Chapter 4.3.1, the flow beneath the bobsleigh is subject to a Venturi effect, where the flow accelerates as the clearance with the ground diminishes. This acceleration generates a low-pressure region, creating a suction effect downwards, increases the aerodynamic downforce acting on the sleigh [25].

Figure 5.6 compares the pressure coefficient distribution on the cowling surface. It can be observed that the pressure gradient in the nose transition to the underside on the *Enhanced Model* is significantly smoother, achieving a 29.78% increase in pressure at the downward spike occurring at approximately $-1\,m$ in the position axis. This improvement is attributed to the increased ground clearance on the *Enhanced Model*.

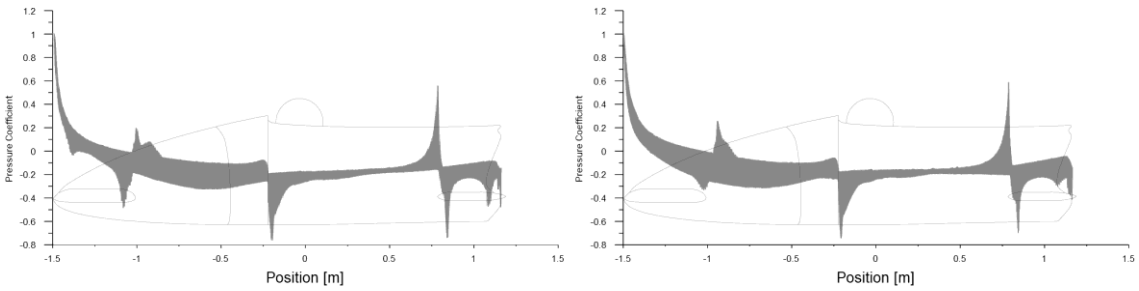

Figure 5.6: Pressure coefficient distribution on the cowling surface for the Reference Model (top) and the Enhanced Model (bottom)

The effects of this modification can also be verified in Figure 5.7. In the *Reference Model*, a rapid pressure rise occurs on the ground surface under the bobsleigh, followed by a sharp drop at the rear end. This behaviour possibly indicates flow stagnation due to a reduced ground clearance.

By increasing the ground clearance, the Enhanced Model allows an earlier pressure increase in the flow stream, resulting in a smoother pressure gradient extending toward the rear end.

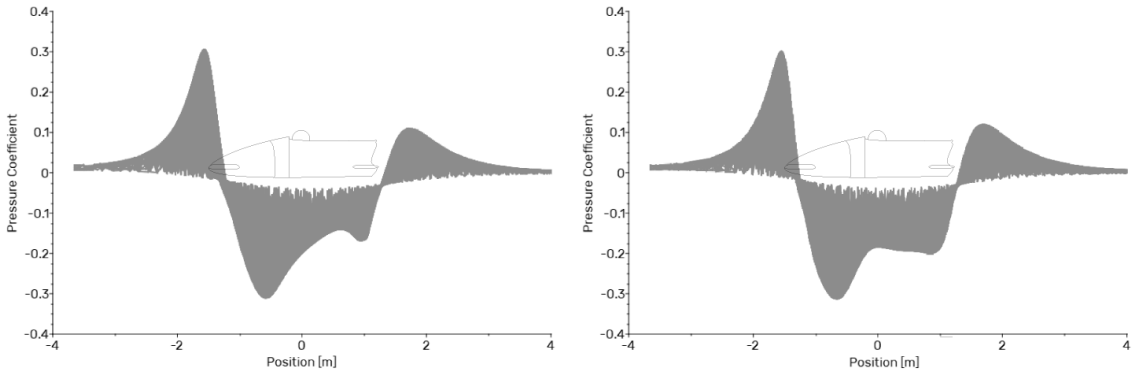

Figure 5.7: Pressure coefficient distribution on the ground surface for the Reference Model (top) and the Enhanced Model (bottom)

The implementation of the diffuser effectively decelerates the flow ejected in the rear of the sleigh, reducing the low-velocity wake area (Figure 5.8). This is further supported by the increase in pressure in the wake region seen in Figure 5.2. In addition to wake reduction, the diffuser raises the flow from the ground, preventing interference with the ice surface and avoiding getting caught in its boundary layer, which would increase skin friction drag on the ground. Moreover, raising the wake promotes a more gradual mixing process downstream, recovering velocity more efficiently and reducing pressure drag.

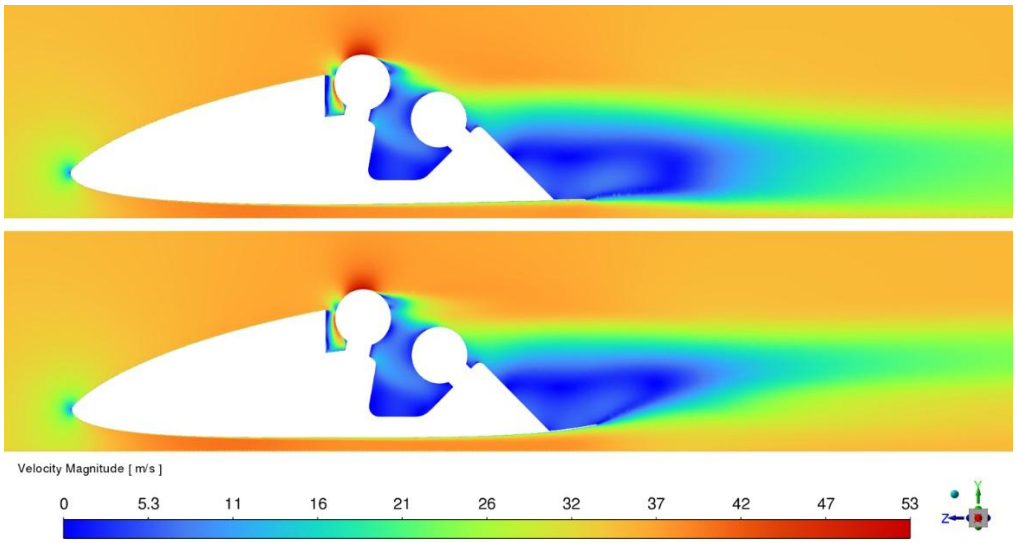

Figure 5.8: Velocity contour on the symmetry plane for the Reference Model (top) and the Enhanced Model (bottom)

5.2.3 Bumpers and Side Walls

The interaction between the airflow and the bumpers is a significant source of aerodynamic disturbance and vortex formation. Flow separation is particularly evident at the transitions between the bumper's leading edge and its middle section, as well as between the middle and trailing edges. As illustrated in Figure 5.9, The *Enhanced Model* vastly reduced separation in the leading edge. Additionally, the *Enhanced Model* minimised flow stagnation along the side wall caused by the front bumper, as seen in Figure 5.10, and redirected it to the rear bumper reducing the velocity of the disturbed flow.

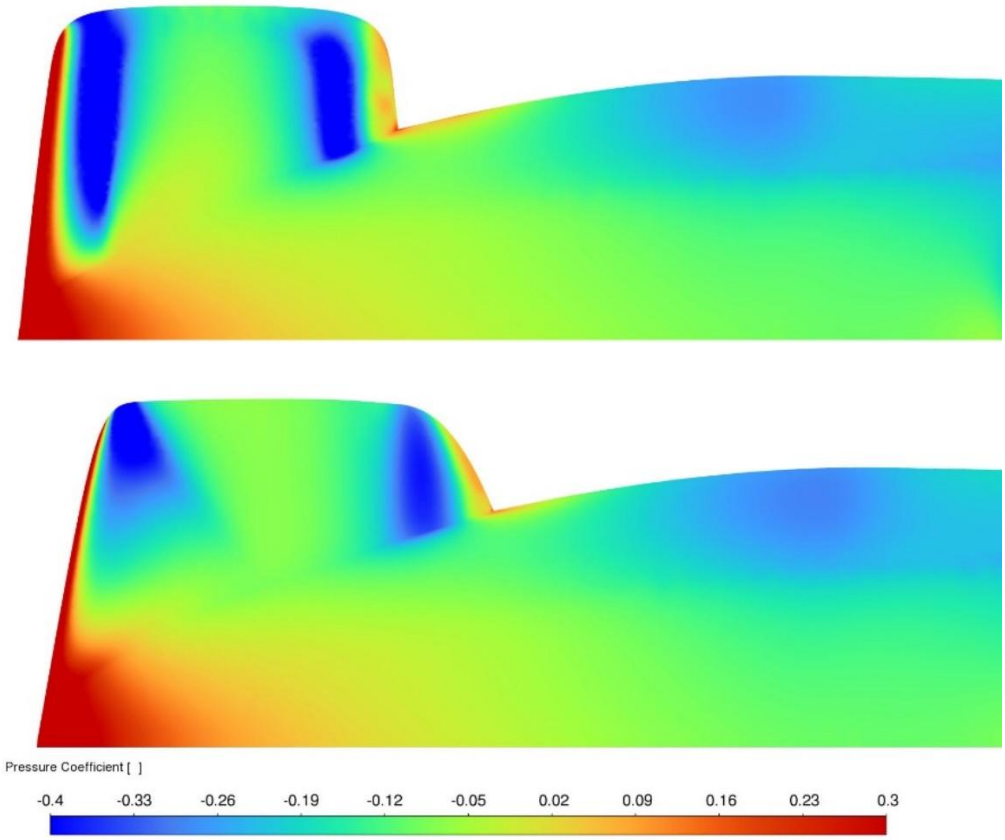

Figure 5.9: Top view of pressure coefficient contour on the bobsleigh surface on the Reference Model (top) and Enhanced Model (bottom)

Also apparent in Figure 5.9 is the separation region occurring in the side, behind the front bumper. All attempts to further streamline this section were unsuccessful, as they improved flow adherence but introduced crippling additional drag.

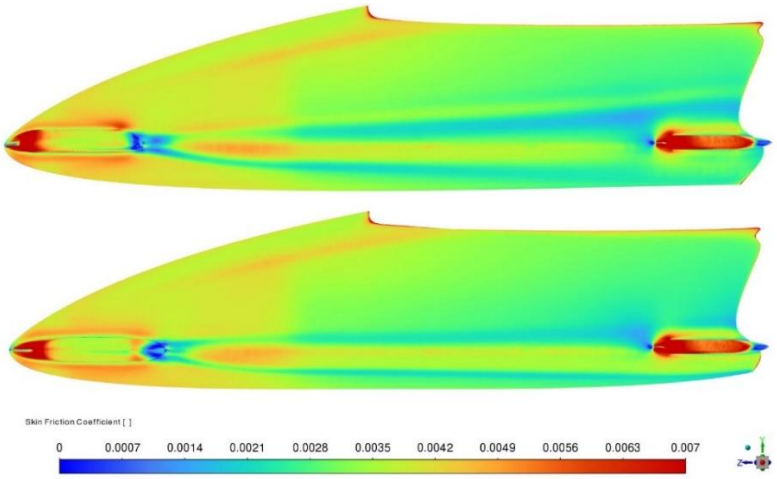

Figure 5.10: Skin friction coefficient contour on the bobsleigh surface on the Reference Model (top) and Enhanced Model (bottom)

5.2.4 Track Straight Sections

All previously discussed results were obtained from simulations that did not account for external confinements near the bobsleigh, interacted only with the bobsleigh surfaces and the ground. While this assumption is valid for certain cornering sections of the track, it cannot be accurately applied to straight sections [24]. In these segments, confining walls positioned close to the sleigh influence flow development and aerodynamic performance.

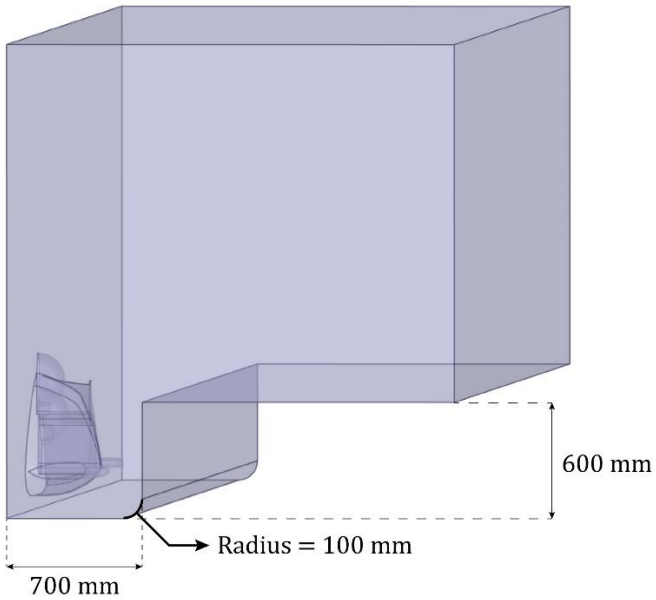

Figure 5.11: Control volume for the straight sections, with cut-out dimensions

Additional simulations were conducted to analyse the aerodynamic effects of the confinement. The respective control volume configuration retained the general dimensions of the initial setup but incorporated a cut-out region representing the presence of a confining wall. The straight section dimensions, shown in Figure 5.11, follow the regulations set in [30]. The resulting blockage of 3.72% ensures that the experienced blockage effects in these simulations are accurate to real phenomena.

The confinement of the space by the walls causes local accelerations due to the Venturi effect, apparent in Figure 5.12, where velocity values were measured in a cross-sectional plane located in the widest part of the cowling. This acceleration increases the high-velocity area surrounding the bobsleigh, significantly reducing pressure in the affected areas.

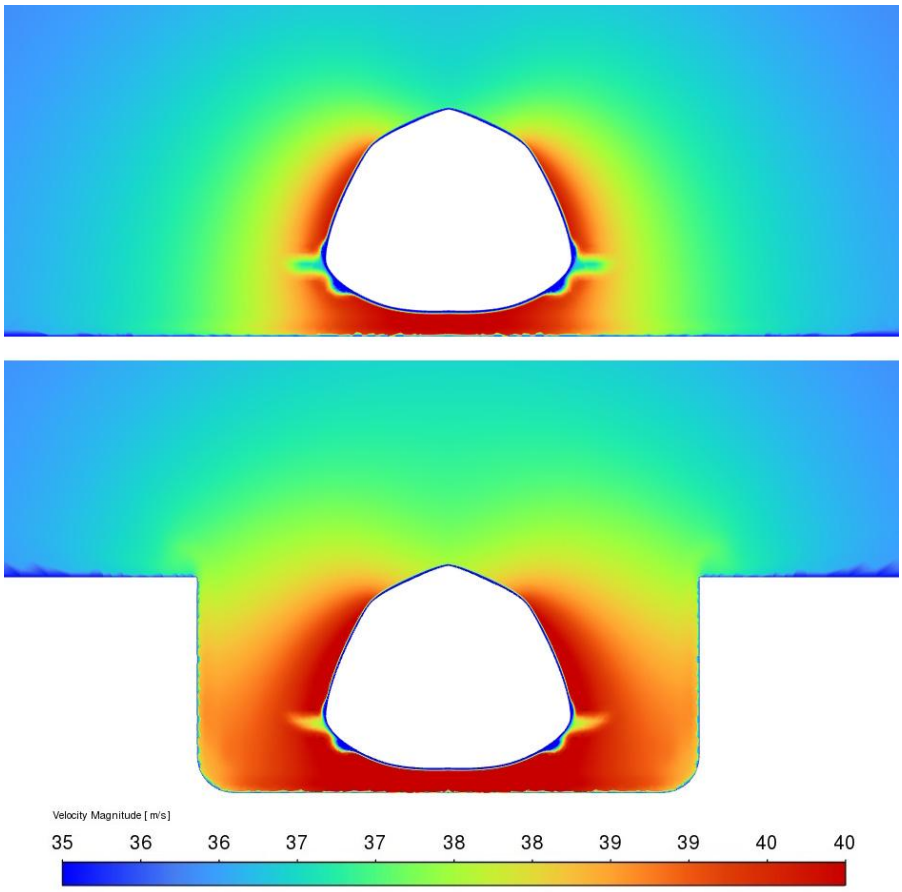

Figure 5.12: Velocity contour on the Enhanced Model surfaces without confining walls (top) and within a straight section (bottom)

Additionally, changes in pressure distribution can be verified in Figure 5.13, where the side walls and cavity in particular experience reduced pressure due to flow acceleration. The blockage effects introduced by the confining walls significantly increases drag generation around the bobsleigh, further deteriorating the aerodynamic performance of the sled.

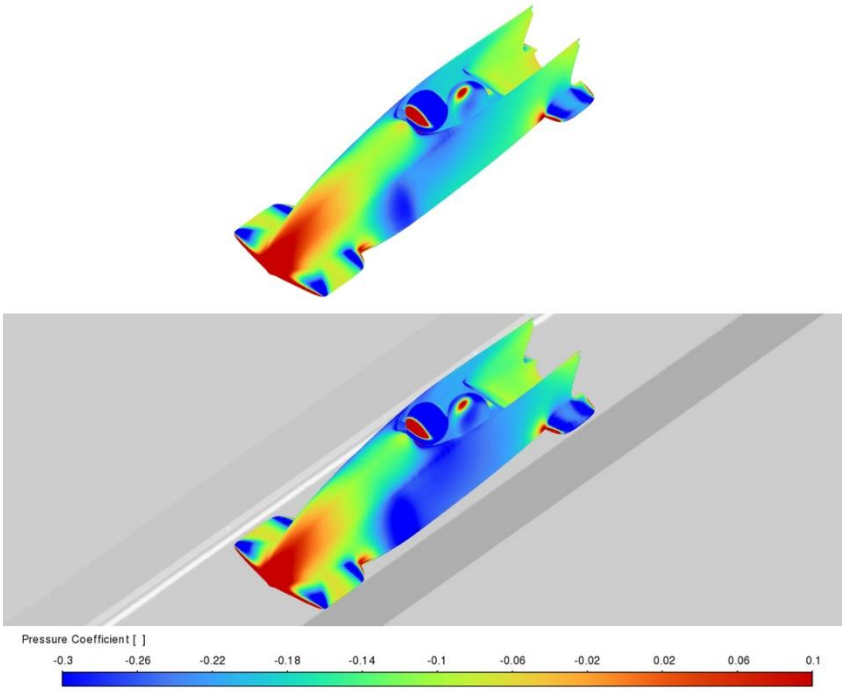

Figure 5.13: Pressure coefficient contour on the Enhanced Model surfaces without confining walls (top) and within a straight section (bottom)

5.3 Aerodynamic Coefficients

This section presents a comprehensive analysis of aerodynamic drag, lift and pitching moment coefficients, comparing their values to assess the effects of design modifications and different flow conditions.

The aerodynamic coefficients for simulations conducted at 35 m/s and 15 m/s are presented in Table 5.1 and Table 5.2, respectively.

Table 5.1: Aerodynamic coefficients for 35 m/s cases

	C_D	C_L	C_M	$A\ (m^2)$
Reference Model	0.21668	−0.08325	−0.02875	0.1928
Enhanced Model	0.20771	−0.19483	−0.03523	0.1876
Enhanced Model (**50 *mm*** clearance)	0.21086	−0.22441	−0.03579	0.1876
Enhanced Model (straight section)	0.22772	−0.26986	−0.02016	0.1876

It is important to note the third case presented in Table 5.1 corresponds to a simulation conducted on the *Enhanced Model*, in which the ground clearance was reduced to 50 mm, matching that of the *Reference Model*. This configuration allowed for an isolated examination of the impact of the ground clearance on drag reduction.

Table 5.2: Aerodynamic coefficients for 15 m/s *cases*

	C_D	C_L	C_M	A
Reference Model	0.22156	−0.05756	−0.02771	0.1928
Enhanced Model	0.21568	−0.20037	−0.03430	0.1876

The *Enhanced Model* effectively reduced both drag coefficient and frontal area, leading to an overall 6.73% decrease in aerodynamic drag at 35 m/s , with 5.31% of this reduction attributed to the increased ground clearance. Additionally, compared to the *Reference Model*, it also increases downforce by 127.72% and pitching moment by 19.23%. While the increase in pitching moment is relatively minor, the significant rise in downforce could potentially enhance runner-to-ice contact, increasing frictional resistance in the ground, slowing down the sleigh.

This effect can be evaluated by comparing maximum speed values in both models. Substituting Equations (3.2) and (3.3) into Equation (3.1), gives:

$$W \sin\theta = F_D + \mu_k(W \cos\theta - F_L) \tag{5.1}$$

Further substituting Equations (3.8) and (3.9):

$$W \sin\theta = \frac{1}{2}C_D \rho V^2 A + \mu_k \left(W \cos\theta - \frac{1}{2}C_L \rho V^2 A\right) \tag{5.2}$$

A comparison between models reveals a 3.14% increase in maximum speed with the *Enhanced Model*.

Finally, as anticipated, the straight section case results in a 9.63% increase in aerodynamic drag, due to flow behaviour alteration introduced by the presence of the confining walls. This configuration also leads to a 38.51% increase in downforce and a 42.77% reduction in pitching moment.

Chapter 6

6 Conclusion

This work has presented a detailed analysis of the aerodynamic phenomena determining bobsleigh performance, using CFD simulations. The simulations employed the Realizable $k-\varepsilon$ turbulence model with Non-Equilibrium Wall Functions for turbulence closure. The set conditions were representative of those during competitive and training runs, allowing for realistic aerodynamic behaviour analysis.

The primary objective of this study was to identify potential design modifications, aiming to improve the aerodynamic efficiency of a bobsleigh. To this end, initial simulations were conducted for the *Reference Model*, designed using photographic references of designs used by high-performance teams in recent competitions. This baseline analysis provided understanding of the flow behaviour, including drag sources and pressure distribution. With the help of existing research, several geometric configurations were explored.

Following an iterative design, the model which showed the most significant aerodynamic improvement was designated the *Enhanced Model*. The aerodynamic characteristics of this improved geometry were compared to those of the *Reference Model* to quantify the effects of the modifications.

The identified most influential design parameters on aerodynamic performance were the front bumper thickness and length, ground clearance distance and diffuser angle. The following modifications were applied:

- **Front bumper redesign:** the new bumper geometry is lengthier and thicker, streamlining its shape, reducing flow separation in its middle section while also reducing stagnation further downstream.
- **Ground clearance adjustment:** ground clearance was increased from $50\,mm$ to $70\,mm$, which reduced the Venturi effect experienced by the flow in the underside, providing a smoother pressure gradient and reduced aerodynamic disturbances in the region.
- **Diffuser optimization: t**he diffuser angle was increased, coupled with a bulky profile, to slow down the wake flow while directing it upward. This adjustment reduced the low-velocity wake region, promoting a more gradual re-mixing with the high-energy free-stream.

As a result of the optimisations, the *Enhanced Model* achieved an overall reduction of 6.37% in drag generation. However, a substantial increase in downforce was also noted, which slightly impacts performance, producing a 3.14% increase in maximum speed.

6.1 Future Work

Given the time and hardware constraints limiting this study, several ways for improvement in future research are suggested:

- **Implementation of the SST $k-\omega$ turbulence model:** This would require much finer mesh configurations and more powerful hardware but would allow a more accurate resolution in near-wall flow, particularly in areas of strong separation.
- **Inclusion of runners and axles on the model:** The current simulations exclude these features, but previous research indicates that significant vortex and drag generation are caused by them. Including these elements would make the flow simulations more representative.
- **Full model simulation:** Including the entirety of the bobsleigh geometry in simulations, without bisecting it with a symmetrical plane, would increase computational cost but would allow for the study of the effects of asymmetric inflow and nose rotation conditions.
- **Wind tunnel testing:** Wind tunnel testing is extensively used to validate CFD results, ensuring their accuracy. Additionally, it could offer a more practical framework for iterative refinement.

References

[1] ‘IBSF | International Bobsleigh & Skeleton Federation: Result’. Accessed: Sep. 27, 2024. [Online]. Available: https://www.ibsf.org/en/result/192800/?cHash=b3fef33bd3d22405d320a9a5e779d949

[2] H.-S. Shim, Y.-N. Lee, and K.-Y. Kim, ‘Optimization of bobsleigh bumper shape to reduce aerodynamic drag’, *Journal of Wind Engineering and Industrial Aerodynamics*, vol. 164, pp. 108–118, May 2017, doi: 10.1016/j.jweia.2017.02.012.

[3] G. Gibertini, A. Soldati, M. Campolo, M. Andreoli, and G. Moretti, ‘Aerodynamic Analysis of a Two-Man Bobsleigh’, in *6th World Congress of Biomechanics (WCB 2010). August 1-6, 2010 Singapore*, vol. 31, C. T. Lim and J. C. H. Goh, Eds., in IFMBE Proceedings, vol. 31. , Berlin, Heidelberg: Springer Berlin Heidelberg, 2010, pp. 228–231. doi: 10.1007/978-3-642-14515-5_59.

[4] H.-S. Shim, H.-Y. Jung, and K.-Y. Kim, ‘Aerodynamic Performance Analysis of a Bobsleigh Body Shape’, in *Volume 7B: Fluids Engineering Systems and Technologies*, Houston, Texas, USA: American Society of Mechanical Engineers, Nov. 2015, p. V07BT09A055. doi: 10.1115/IMECE2015-54168.

[5] F. Motallebi, P. Dabnichki, and D. Luck, ‘Advanced bobsleigh design. Part 2: aerodynamic modifications to a two-man bobsleigh’, vol. 218, 2004.

[6] H. Chowdhury, B. Loganathan, F. Alam, and H. Moria, ‘Aerodynamic Body Position of the Brakeman of a 2-man Bobsleigh’, *Procedia Engineering*, vol. 112, pp. 424–429, 2015, doi: 10.1016/j.proeng.2015.07.219.

[7] M. da S. de Vasconcelos, ‘Estudo Aerodinâmico Preliminar de um Bobsled de 2 Lugares’, University of Beira Interior - FE Departamento de Ciências Aeroespaciais, 2023.

[8] M. Vaza, ‘Procuram-se portugueses fortes e rápidos para conduzir um trenó’, PÚBLICO. Accessed: Apr. 05, 2025. [Online]. Available: https://www.publico.pt/2014/02/07/desporto/noticia/procuramse-portugueses-fortes-e-rapidos-para-conduzir-um-treno-1622689

[9] ‘About’, Bobteam Portugal. Accessed: Apr. 05, 2025. [Online]. Available: https://bobteamportugal.pt/about/

[10] ‘Home’, Bobteam Portugal. Accessed: Apr. 05, 2025. [Online]. Available: https://bobteamportugal.pt/

[11] ‘IBSF | International Bobsleigh & Skeleton Federation: Bobsleigh’. Accessed: Sep. 30, 2024. [Online]. Available: https://www.ibsf.org/en/our-sports/bobsleigh

[12] A. D. Lopes and S. R. Alouche, ‘Two-Man Bobsled Push Start Analysis’, *Journal of Human Kinetics*, vol. 50, no. 1, pp. 63–70, Apr. 2016, doi: 10.1515/hukin-2015-0143.

[13] ‘Technique - BBSA’. Accessed: Oct. 31, 2024. [Online]. Available: https://www.thebbsa.co.uk/the-sports/bobsleigh/technique/

[14] P. Dabnichki, F. Motallebi, and E. Avital, ‘Advanced bobsleigh design. Part 1: body protection, injury prevention and performance improvement’, vol. 218, 2004.

[15] ‘The perfect slide: The science of bobsledding’, Smithsonian Science Education Center. Accessed: Oct. 20, 2024. [Online]. Available: https://ssec.si.edu/stemvisions-blog/perfect-slide-science-bobsledding

[16] ‘Hunt for Gold in High-Tech Bobsled’. Accessed: Nov. 10, 2024. [Online]. Available: https://www.schaeffler.com/en/media/stories/technology-system-stories/winter-sports-high-tech-bob/

[17] ‘The Start and Drive’, Team Bobsleigh Brad. Accessed: Oct. 18, 2024. [Online]. Available: https://www.teambobsleighbrad.com/the-start-and-drive

[18] ‘Bobsledding | History, Rules, & Facts | Britannica’. Accessed: Sep. 30, 2024. [Online]. Available: https://www.britannica.com/sports/bobsledding

[19] ‘Saint Moritz Bobsleigh Club’. Accessed: Sep. 30, 2024. [Online]. Available: http://www.bobclub-stmoritz.ch/125-years

[20] ‘From St. Moritz Streets to Olympic Glory: The Journey of Bobsleigh - Olympic Stage’. Accessed: Oct. 01, 2024. [Online]. Available: https://www.keystage2literacy.co.uk/bobsleigh/

[21] ‘Winter Olympics Technology’, HISTORY. Accessed: Oct. 01, 2024. [Online]. Available: https://www.history.com/topics/sports/winter-olympics-technology-1

[22] ‘International Bobsleigh Rules 2024’. IBSF, Sep. 2024. [Online]. Available: https://www.ibsf.org/fileadmin/user_upload/Resources/Sports/Rules_Quotas/2024_International_Rules_BOBSLEIGH.pdf

[23] *IBSF World Cup Yanqing: 2-man bobsleigh 1st heat*, (Nov. 17, 2023). Accessed: Nov. 11, 2024. [Online Video]. Available: https://www.cbc.ca/player/play/video/1.7031222

[24] M. Estivalet and P. Brisson, *The Engineering of Sport 7: Vol. 2*. Paris: Springer Paris, 2008. doi: 10.1007/978-2-287-09413-2.

[25] O. Lewis, 'Aerodynamic analysis of a 2-man bobsleigh', Master of Science Thesis, Delft University of Technology - Faculty of Aerospace Engineering, 2006.

[26] M. Komarova, 'World Bobsleigh Tracks: from Geometry to the Architecture of Sports Facilities', *Nexus Netw J*, vol. 20, no. 1, pp. 235–249, Apr. 2018, doi: 10.1007/s00004-017-0348-6.

[27] E. Sabbioni, S. Melzi, F. Cheli, and F. Braghin, 'Chapter 7: Bobsleigh and Skeleton', in *The Engineering Approach to Winter Sports*, F. Braghin, F. Cheli, S. Maldifassi, S. Melzi, and E. Sabbioni, Eds., Springer New York, 2015.

[28] S. Magazine and N. Geiling, 'India's Dying Well of Death', Smithsonian Magazine. Accessed: Nov. 07, 2024. [Online]. Available: https://www.smithsonianmag.com/travel/indias-well-death-1-180954126/

[29] 'IBSF Bobsled and Skeleton World Championships | Lake Placid, NY 12946'. Accessed: Nov. 07, 2024. [Online]. Available: https://www.iloveny.com/event/ibsf-bobsled-and-skeleton-world-championships/69624/

[30] 'IBSF Track Rules 2019'. Accessed: Nov. 06, 2024. [Online]. Available: https://www.ibsf.org/fileadmin/user_upload/Resources/Sports/Rules_Quotas/IBSF_Track_Rules_am2019.pdf

[31] J. O. Hinze, *Turbulence*. in McGraw-Hill Classic Textbook Reissue. McGraw-Hill, 1975.

[32] F. M. White and H. Xue, *Fluid mechanics*, Ninth edition. New York, NY: McGraw-Hill, 2021.

[33] S. B. Pope, *Turbulent flows*, First Edition, Tenth Printing. Cambridge: Cambridge Univ. Press, 2015.

[34] T. L. Bergman and F. P. Incropera, Eds., *Fundamentals of Heat and Mass Transfer*, 7th ed. Hoboken, NJ: Wiley, 2011.

[35] 'Law of the wall', *Wikipedia*. Nov. 29, 2024. Accessed: Feb. 07, 2025. [Online]. Available: https://en.wikipedia.org/w/index.php?title=Law_of_the_wall&oldid=1260174983

[36] J. D. Anderson, *Computational Fluid Dynamics: The Basics with Applications*. in McGraw-Hill International Editions: Mechanical Engineering. McGraw-Hill, 1995.

[37] N. A. Che Sidik, S. N. A. Yusuf, Y. Asako, S. B. Mohamed, and W. M. A. Aziz Japa, 'A Short Review on RANS Turbulence Models', *CFDL*, vol. 12, no. 11, pp. 83–96, Nov. 2020, doi: 10.37934/cfdl.12.11.8396.

[38] 'K-epsilon models -- CFD-Wiki, the free CFD reference'. Accessed: Feb. 10, 2025. [Online]. Available: https://www.cfd-online.com/Wiki/K-epsilon_models

[39] M. Blakeslee, 'Wilcox k-ω Model'. Accessed: Feb. 10, 2025. [Online]. Available: https://help.altair.com/hwcfdsolvers/acusolve/topics/acusolve/training_manual/wilcox_k_model_r.htm

[40] 'SST k-omega model -- CFD-Wiki, the free CFD reference'. Accessed: Feb. 10, 2025. [Online]. Available: https://www.cfd-online.com/Wiki/SST_k-omega_model

[41] A. Winkler, A. Pernpeintner, and M. Estivalet, 'Improving the Performance of a Bobsleigh by Aerodynamic Optimization (P212)', in *The Engineering of Sport 7: Vol. 2*, Paris: Springer Paris, 2009, pp. 329–338. doi: 10.1007/978-2-287-09413-2_41.

[42] A. Pernpeintner and A. Winkler, 'Lessons learned from the aerodynamic shape development process of a bobsleigh', *Procedia Engineering*, vol. 2, no. 2, pp. 2407–2412, Jun. 2010, doi: 10.1016/j.proeng.2010.04.007.

[43] 'Friedrich with 2-man bobsleigh victory in St. Moritz now World Cup record winner'. Accessed: Nov. 12, 2024. [Online]. Available: https://www.ibsf.org/en/news/detail/friedrich-with-2-man-bobsleigh-victory-in-st-moritz-now-world-cup-record-winner

[44] '2022/23 North American Cup: Men's and Women's Skeleton, Men's 2-Man Bobsleigh and Women's Monobob | Adirondacks', ADK Taste - The Best of the Adirondacks. Accessed: Nov. 12, 2024. [Online]. Available: https://www.adktaste.com/adirondack-events/events-north-american-cup-bobsleigh-monobob-december-2

[45] Choi, Chang-Koon and Kwon, Dae-Kun, 'Wind tunnel blockage effects on aerodynamic behavior of bluff body', *Wind and Structures*, vol. 1, no. 4, pp. 351–364, Dec. 1998, doi: 10.12989/WAS.1998.1.4.351.

[46] 'Continuity Equation'. Accessed: Mar. 11, 2025. [Online]. Available: https://www.princeton.edu/~asmits/Bicycle_web/continuity.html

[47] 'A Comparison of ANSYS Fluent Meshing and Ansys Meshing for CFD - PADT'. Accessed: Feb. 11, 2025. [Online]. Available: https://www.padtinc.com/2021/05/11/comparison-ansys-fluent-meshing-ansys-meshing-cfd/

[48] ‘Y+ and Grid Types - MR CFD’. Accessed: Feb. 17, 2025. [Online]. Available: https://www.mr-cfd.com/y-and-grid-types/

[49] ‘Better meshing using ANSYS Fluent Meshing?’ Accessed: Feb. 17, 2025. [Online]. Available: https://www.linkedin.com/pulse/better-meshing-using-ansys-fluent-hashan-mendis

[50] ‘What is y+ (yplus)? - Using SimScale / Fluid Flow / CFD’, SimScale CAE Forum. Accessed: Feb. 07, 2025. [Online]. Available: https://www.simscale.com/forum/t/what-is-y-yplus/82394

[51] J. Abrahamson, *Fluent Theory Guide*. Canonsburg, PA: ANSYS, Inc., 2023.

Appendices

A Boundary Conditions

inlet	
Condition	velocity-inlet
Velocity Magnitude	15 m/s or 35 m/s; depending on the case
Turbulent Intensity	0.5 %
Turbulent Viscosity Ratio	2
outlet	
Condition	pressure-outlet
Turbulent Intensity	0.5 %
Turbulent Viscosity Ratio	2
free-slip wall	
Condition	Specified Shear [Pa]: 0 (all directions)
Motion	Stationary Wall
floor	
Condition	No Slip
Motion	Moving Wall (15 m/s or 35 m/s; depending on the case)
symmetry	
Condition	symmetry
bobsleigh	
Condition	No Slip
Motion	Stationary Wall